ALMA MATER STUDIORUM
UNIVERSITÀ DI BOLOGNA

DEPARTMENT OF PHYSICS AND ASTRONOMY "A. RIGHI"

SECOND CYCLE DEGREE

PHYSICS

Embedding the Axio-Chameleon Screening of Fifth-Forces into String Theory

Supervisor
Prof. Michele Cicoli

Co-supervisor
Prof. Susha Louise Parameswaran

Defended by
Giacomo Micheli

Graduation Session September 2025

Academic Year 2024/2025

Abstract

Light scalar fields are ubiquitous in beyond the Standard Model and string constructions, but they naively induce unobserved fifth-forces. Axio-chameleon screening [1] has recently been proposed as a promising mechanism to explain the absence of these fifth-forces, and the goal of this thesis is to embed it in String Theory. In particular, a good contender seems to be a D3/$\overline{\text{D3}}$-brane moving on a warped deformed conifold along both the radial and some angular directions. In the model presented here, the Standard Model is assumed to live on the brane and the radial brane-position modulus couples to it as a Quasi-Brans-Dicke scalar through the warp factor. This can be interpreted as a Quintessence field and the screening mechanism provides justification for the lack of observable fifth-forces in solar-system experiments.

Contents

Conventions

Metric signature: $(-,+,+,+)$

Fields mass dimension: $[\phi] = 0$

Einstein-Hilbert action: $S_{\text{EH}} = +\frac{M_p^2}{2}\int d^n x\sqrt{-g_n}R_n$

Planck mass-length relation: $M_p = \frac{1}{l_p}$

String mass-length relation: $M_s = \frac{2\pi}{l_s} = \frac{1}{\sqrt{\alpha'}}$

10D gravitational coupling: $2\kappa^2 = (2\pi)^7(\alpha')^4$

1 Introduction

The lack of observable evidence for fifth-forces is one of the main constraints in the formulation of cosmological models involving additional scalar fields on top of the Standard Model (SM). Post-Newtonian tests of gravity performed within the solar system rely on the observable L defined as

$$\phi_{\text{ext}}(r) = \phi_\infty - \frac{L}{r} \,, \tag{1}$$

where ϕ_{ext} is the scalar field outside of a spherically symmetric astrophysical object, like the Sun, with asymptotic value ϕ_∞.

Screening mechanisms relax experimental constraints from unobserved fifth-forces by introducing a matter-density dependence for some parameters of the field, such as its mass or its coupling constant with the SM. In particular, the axio-chameleon mechanism described in [1] manages to reduce L by considering a saxion-axion couple interacting through the generalized kinetic term

$$\mathcal{L} \supset -\sqrt{-g}\frac{f^2}{2}\mathcal{G}_{ab}(\phi)\partial_\mu\phi^a\partial^\mu\phi^b \,, \tag{2}$$

where f is a scale factor of mass dimension 1. This is a totally novel mechanism which cannot be reduced to single-field screening due to the fact that the metric in (2) cannot be diagonalized in general.

Taking the saxion to be a Quasi-Brans-Dicke (QBD) scalar has the additional merit of automatically ensuring the validity of the Equivalence Principle, which stands on extremely firm experimental ground. One does so by coupling it to the Standard Model only through a Weyl rescaling of the metric. The original paper assumes the rescaling to be of the form

$$\tilde{g}_{\mu\nu} = A^2(\phi)g_{\mu\nu} = e^{2\mathfrak{g}\phi}g_{\mu\nu} \,, \tag{3}$$

where $\mathfrak{g}$ is a constant. In this thesis, we broaden the discussion to generic Weyl factors.

In addition, we embed the axio-chameleon mechanism in String Theory. We imagine the SM to live on a D3/ $\overline{\text{D3}}$-brane moving on a warped deformed conifold on both the radial and some angular directions. By taking the warp factor, which depends on the radial direction, as our Weyl factor, we manage to couple the radial-position modulus to the SM as a QBD scalar. The angular coordinates, or combinations of them, are assumed to act as axions, forming a saxion-axion pair and making the screening mechanism possible. To be more precise, by taking the 4D SM metric as the pull-back of the 10D Einstein-frame metric, we end up with a disformal transformation

$$\tilde{g}_{\mu\nu} = A^2(\phi)g_{\mu\nu} + B(\phi)\mathcal{G}_{ab}(\phi)\partial_\mu\phi^a\partial_\nu\phi^b \,. \tag{4}$$

This can be effectively brought back to a conformal transformation for non-relativistic matter only if the scalar fields are static, as we analyze.

The saxion-SM interaction generates a source term in the saxion equation of motion, which cannot be solved analytically in general. We approximate the Solar System matter distribution with the Sun alone, assuming it to have uniform density, and use numerical techniques to approximate the system total energy E_{tot}. Finding it dependent on the field integration parameter ϕ_s, we minimize it with respect to it and finally quantify the amount of screening through the ratio L/L_0, where L_0 is the post-Newtonian parameter without screening applied.

In Chapter 2, the reader finds a comprehensive summary of the effective Supergravity theory arising from type IIB String Theory. We focus in particular on the Einstein-Hilbert (EH) and Dirac actions, highlighting the emergence of brane-position moduli from compactification. We mention axions and their properties and conclude with an introduction to conifold geometries. Chapter 3 consists of an overview on QBD theories, as well as on fifth-forces sourced by these. We also describe both single-field and the axio-chameleon screening mechanisms. Chapter 4 presents original research, providing attempted embeddings of the axio-chameleon screening mechanism in String Theory, using both closed-string and brane-position moduli. We focus mostly on the latter, since it is far more promising. We believe this novel mechanism could be relevant in cosmological models where one takes the radial modulus as a Quintessence field. Therefore, we provide a short overview on Quintessence in the Appendix, together with a discussion on fictitious non-linear sigma models.

2 Type IIB String Theory

It is a well-known result that low-energy string theories effectively produce 10D supergravity theories. We start our discussion here, focusing in particular on the bosonic sector of the type IIB theory (see [2] for an extensive review). In the Einstein frame, the closed string effective action is

$$\begin{aligned} S = \frac{1}{2\kappa^2}\int d^{10}X\sqrt{-G}\left(R_{10} - \frac{|\partial\tau|^2}{2(\mathsf{Im}(\tau))^2} - \frac{|G_3|^2}{2\mathsf{Im}(\tau)} - \frac{|\tilde{F}_5|^2}{4}\right) \\ - \frac{i}{8\kappa^2}\int \frac{C_4\wedge G_3\wedge \bar{G}_3}{\mathsf{Im}(\tau)}\,, \end{aligned} \tag{5}$$

where G and R_{10} are the 10D Einstein metric and Ricci scalar respectively,

$$\tau \equiv C_0 + ie^{-\Phi} \tag{6}$$

is the axiodilaton,

$$G_3 \equiv F_3 - \tau H_3\,, \tag{7}$$

$$F_3 \equiv \mathsf{d}C_2\,, \tag{8}$$

$$H_3 \equiv \mathsf{d}B_2\,, \tag{9}$$

$$F_5 \equiv \mathsf{d}C_4 \tag{10}$$

and

$$\tilde{F}_5 \equiv F_5 - \frac{1}{2}C_2\wedge H_3 + \frac{1}{2}B_2\wedge F_3 \tag{11}$$

are fluxes, with $\tilde{F}_5 \equiv \star\tilde{F}_5$ to impose self-duality. The C_0, C_2 and C_4 are even-dimensional forms coming from the R-R sector, which are characteristic of type IIB string theory, while B_2 comes from the NS-NS sector and is shared with type IIA. Finally,

$$2\kappa^2 \equiv (2\pi)^7(\alpha')^4\,. \tag{12}$$

In (5) one can recognize the 10D Einstein-Hilbert term, which is going to be of extreme relevance for us in the upcoming discussion. However, before that, let us briefly recall that type IIB string theory also admits additional localized objects charged under the R-R forms: D-branes. These are the loci where open strings end. A Dp-brane has p spatial dimensions and is charged under C_{p+1} via the Chern-Simons action

$$S_{\mathsf{CS}} = i\mu_p\int_{\Sigma_{p+1}}\sum_n C_n\wedge e^{\mathcal{F}}\,, \tag{13}$$

where Σ_{p+1} is the Dp-brane worldvolume, μ_p is the brane charge and

$$\mathcal{F}_{ab} \equiv B_{ab} + 2\pi\alpha' F_{ab} \tag{14}$$

represents interactions with the closed string background. In (14), B_{ab} is the pullback of B_{MN} on the brane worldvolume.

Together with (13), one must also consider the Dirac-Born-Infeld action

$$S_{\mathsf{DBI}} = -g_s T_p \int d^{p+1}\sigma e^{-\Phi} \sqrt{-\mathsf{det}(G_{ab} + \mathcal{F}_{ab})}\,, \tag{15}$$

where T_p is the brane tension, G_{ab} is the pullback of the 10D metric on the brane worldvolume and F_{ab} plays the same role as in (13). Neglecting fluxes, (15) simplifies into the Dirac action. One can express μ_p and T_p through fundamental quantities using

$$\mu_p = \pm g_s T_p \tag{16}$$

for a brane/anti-brane and

$$T_p = \frac{1}{(2\pi)^p g_s (\alpha')^{\frac{p+1}{2}}} = \frac{2\pi}{g_s l_s^{p+1}}\,. \tag{17}$$

In the end, the open string bosonic sector consists of the gauge field A_a associated to the field strength F_{ab} and scalar fields representing fluctuations of the brane position.

The EH and Dirac terms are going to be the object of our attention for the next two sections. In particular, we are going to study their behavior under compactification, splitting the 10D metric as [3]

$$ds_{10}^2 = h^{-\frac{1}{2}}(y) e^{2\omega(x)} g_{\mu\nu} dx^\mu dx^\nu + h^{\frac{1}{2}}(y) \mathcal{V}^{\frac{1}{3}}(x) g_{mn} dy^m dy^n\,, \tag{18}$$

where $h(y)$ is the warp factor, $\mathcal{V}$ is the dimensionless compactified volume, g_{mn} is the 6D metric of the compact space defined such that

$$\int d^6 y \sqrt{g_6} = l_s^6 \tag{19}$$

and $\omega(x)$ represents some preserved rescale freedom and will be fixed once we go to the 4D Einstein frame.

2.1 The Einstein-Hilbert action

Let us start from the 10D EH action

$$S_{\mathsf{EH}} = \frac{1}{2\kappa^2} \int d^{10} X \sqrt{-G} R_{10}\,; \tag{20}$$

our goal is to express the volume element and the Ricci scalar in terms of their 4D counterparts. We start from the former. From (18), one can write the 10D metric as

$$G_{MN} = \begin{pmatrix} h^{\frac{1}{2}} e^{-2\omega} g_{\mu\nu} & 0 \\ 0 & h^{-\frac{1}{2}} \mathcal{V}^{-\frac{1}{3}} g_{mn} \end{pmatrix} . \tag{21}$$

Using the determinant property

$$\det \begin{pmatrix} A & 0 \\ 0 & B \end{pmatrix} = \det(A) \det(B) \tag{22}$$

we obtain

$$\begin{aligned} \det(G_{MN}) &= \det \left(h^{-\frac{1}{2}} e^{2\omega} g_{\mu\nu} \right) \det \left(h^{\frac{1}{2}} \mathcal{V}^{\frac{1}{3}} g_{mn} \right) \\ &= \left(h^{-\frac{1}{2}} e^{2\omega} \right)^4 \det(g_{\mu\nu}) \left(h^{\frac{1}{2}} \mathcal{V}^{\frac{1}{3}} \right)^6 \det(g_{mn}) \\ &= h e^{8\omega} \mathcal{V}^2 \det(g_{\mu\nu}) \det(g_{mn}) \end{aligned} \tag{23}$$

and finally

$$\sqrt{-G} = h^{\frac{1}{2}} e^{4\omega} \mathcal{V} \sqrt{g_6} \sqrt{-g_4} . \tag{24}$$

Moving on to the Ricci scalar, we can use the fact that it scales as the inverse metric to write

$$R_{10} \sim G^{MN} = \begin{pmatrix} h^{\frac{1}{2}} e^{-2\omega} g^{\mu\nu} & 0 \\ 0 & h^{-\frac{1}{2}} \mathcal{V}^{-\frac{1}{3}} g^{mn} \end{pmatrix} \tag{25}$$

and

$$R_4 \sim g^{\mu\nu} . \tag{26}$$

From the top-left element in (25), we deduce that

$$R_{10} \supset h^{\frac{1}{2}} e^{-2\omega} R_4 . \tag{27}$$

Together, (24) and (27) give

$$\sqrt{-G} R_{10} \supset h e^{2\omega} \mathcal{V} \sqrt{g_6} \sqrt{-g_4} R_4 . \tag{28}$$

Staring from (20), using (28) and splitting the integral along spacetime and compactified coordinates gives

$$\begin{aligned} S_{\text{EH}} &\supset \frac{1}{2\kappa^2} \int d^4x \sqrt{-g_4} e^{2\omega(x)} \left(\mathcal{V} \int d^6y \sqrt{g_6} h(y) \right) R_4 \\ &= \frac{M_p^2}{2} \int d^4x \sqrt{-g_4} R_4 . \end{aligned} \tag{29}$$

We used our conformal freedom to define

$$e^{2\omega(x)} \equiv \frac{\mathcal{V}_W^0 l_s^6}{\mathcal{V} \int d^6y \sqrt{g_6} h(y)} = \frac{\mathcal{V}_W^0}{\mathcal{V}_W} \,, \tag{30}$$

where $\mathcal{V}_W$ is the warped dimensionless volume and we chose $\mathcal{V}_W^0$ such that

$$M_p^2 = \frac{\mathcal{V}_W^0 l_s^6}{\kappa^2} = \frac{4\pi \mathcal{V}_W^0}{l_s^2} \,. \tag{31}$$

2.2 The Dirac action

Looking now at the DBI action (15), we consider the specific case of a D3/$\overline{\text{D3}}$-brane, ignoring fluxes and assuming the dilaton Φ to be stabilized at its minimum, so that we find the Dirac action

$$S_{\text{D}} = -T_3 \int d^4x \sqrt{-\tilde{g}_4} \,, \tag{32}$$

where the brane tension $T_3 = 2\pi/(g_s l_s^4)$ is evaluated using (17). Recall that in (32) $\tilde{g}_{\mu\nu}$ is the pullback of G_{MN}, i.e.

$$\begin{aligned} \tilde{g}_{\mu\nu} &= \frac{\partial X^M}{\partial x^\mu} \frac{\partial X^N}{\partial x^\nu} G_{MN} = G_{\mu\nu} + \frac{\partial y^m}{\partial x^\mu} \frac{\partial y^n}{\partial x^\nu} G_{mn} \\ &= h^{-\frac{1}{2}} e^{2\omega} g_{\mu\nu} + h^{\frac{1}{2}} \mathcal{V}^{\frac{1}{3}} \frac{\partial y^m}{\partial x^\mu} \frac{\partial y^n}{\partial x^\nu} g_{mn} \,, \end{aligned} \tag{33}$$

where we used the static gauge

$$X^M = \{x^\mu, y^m\} \,. \tag{34}$$

(33) highlights how the the 4D warped metric $\tilde{g}_{\mu\nu}$ and the 4D unwarped metric $g_{\mu\nu}$ are related by a disformal transformation, which differs from a conformal one because of its second term.

Similarly to what we did for the EH term, we aim at expressing the volume element in terms of $g_{\mu\nu}$. Using the determinant properties

$$\det(AB) = \det(A) \det(B) \tag{35}$$

and

$$\det(I + A) \supset 1 + \text{Tr} A \tag{36}$$

we find that

$$\begin{aligned}
\det(\tilde{g}_{\mu\nu}) &= \det\left(h^{-\frac{1}{2}}e^{2\omega}g_{\mu a}\left(\delta^a_\nu + he^{-2\omega}\mathcal{V}^{\frac{1}{3}}g^{ab}\frac{\partial y^m}{\partial x^b}\frac{\partial y^n}{\partial x^\nu}g_{mn}\right)\right) \\
&\supset \det\left(h^{-\frac{1}{2}}e^{2\omega}g_{\mu a}\right)\left(1+\mathrm{Tr}\left(he^{-2\omega}\mathcal{V}^{\frac{1}{3}}g^{ab}\frac{\partial y^m}{\partial x^b}\frac{\partial y^n}{\partial x^\nu}g_{mn}\right)\right) \\
&= \left(h^{-\frac{1}{2}}e^{2\omega}\right)^4\det(g_{\mu a})\left(1+he^{-2\omega}\mathcal{V}^{\frac{1}{3}}\mathrm{Tr}\left(g^{ab}\frac{\partial y^m}{\partial x^b}\frac{\partial y^n}{\partial x^\nu}g_{mn}\right)\right) \\
&= h^{-2}e^{8\omega}\det(g_{\mu a})\left(1+he^{-2\omega}\mathcal{V}^{\frac{1}{3}}g^{ab}\frac{\partial y^m}{\partial x^b}\frac{\partial y^n}{\partial x^a}g_{mn}\right) \\
&= h^{-2}e^{8\omega}\det(g_{\mu\nu})\left(1+he^{-2\omega}\mathcal{V}^{\frac{1}{3}}g^{mn}\partial_\mu y^m\partial^\mu y^n\right)
\end{aligned} \tag{37}$$

and consequently

$$\begin{aligned}
\sqrt{-\det(\tilde{g}_{\mu\nu})} &= \sqrt{-\det(g_{\mu\nu})}h^{-1}e^{4\omega}\left(1+he^{-2\omega}\mathcal{V}^{\frac{1}{3}}g_{mn}\partial_\mu y^m\partial^\mu y^n\right)^{\frac{1}{2}} \\
&\simeq \sqrt{-\det(g_{\mu\nu})}h^{-1}e^{4\omega}\left(1+\frac{1}{2}he^{-2\omega}\mathcal{V}^{\frac{1}{3}}g_{mn}\partial_\mu y^m\partial^\mu y^n\right) \\
&= \sqrt{-\det(g_{\mu\nu})}\left(h^{-1}e^{4\omega}+\frac{1}{2}e^{2\omega}\mathcal{V}^{\frac{1}{3}}g_{mn}\partial_\mu y^m\partial^\mu y^n\right) \\
&= \sqrt{-\det(g_{\mu\nu})}\left(h^{-1}\left(\frac{\mathcal{V}^0_W}{\mathcal{V}_W}\right)^2+\frac{1}{2}\frac{\mathcal{V}^0_W}{\mathcal{V}_W}\mathcal{V}^{\frac{1}{3}}g_{mn}\partial_\mu y^m\partial^\mu y^n\right) .
\end{aligned} \tag{38}$$

It follows that (32) can be rewritten as (see also [4][5])

$$S_{\mathrm{D}} = -\frac{2\pi}{g_s l_s^4}\int d^4x\sqrt{-\det(g_{\mu\nu})}\left(h^{-1}\left(\frac{\mathcal{V}^0_W}{\mathcal{V}_W}\right)^2+\frac{1}{2}\frac{\mathcal{V}^0_W}{\mathcal{V}_W}\mathcal{V}^{\frac{1}{3}}g_{mn}\partial_\mu y^m\partial^\mu y^n\right) . \tag{39}$$

Interestingly, the compactified coordinates y^m have assumed the role of scalar fields, which are referred to as brane-position moduli. In (39), we can recognize both a potential and a generalized kinetic term, where the fields are coupled through the unwarped 6D metric g_{mn}. It is this last term that is going to be responsible for the interesting phenomenology we are analyzing in Chapter 4; therefore, we drop the potential from now on.

2.3 Interactions with the Standard Model

Although one need intersecting stacks of branes for non-abelian gauge symmetries to emerge, assuming the Standard Model to live on a D3/$\overline{\text{D3}}$-brane is a common simplification [6] (see [7] for a model where Dark Matter lives on the D-brane). Following this

toy model ourselves, we can infer relevant information on the interaction between the well-known SM fields and the brane-position moduli.

Let us start by observing that Poincaré invariance forces the brane to be space-time filling, since the opposite would create a distinction among the spacetime coordinates. It follows that the brane lives on the Calabi-Yau as a dimensionless point. Higher-dimensional branes would, instead, have spare dimensions to wrap around cycles of the compact manifold.

A SM localized on the brane will feel the pullback metric evaluated at that point, introducing a dependence on the brane-position moduli through (33). In symbols

$$S_{\text{SM}} = S_{\text{SM}}(\tilde{g}_{\mu\nu}, \psi) \,, \tag{40}$$

where we use ψ to represent the usual SM fields. As we have already stated, (33) is a disformal transformation relating $\tilde{g}_{\mu\nu}$ and $g_{\mu\nu}$. While interesting considerations can be made even in this general case [8], here we decide to take the non-relativistic limit, where (33) can effectively be reduced to a conformal transformation

$$\tilde{g}_{\mu\nu} = h^{-\frac{1}{2}} e^{2\omega} g_{\mu\nu} \tag{41}$$

when studying the coupling of static scalars to the SM [9].

Let us see how in a simplified example. While a conformal relation couples the SM to the scalars (as we will see in details at the beginning of Chapter 3), a purely disformal one couples it to the moduli derivative. For instance, considering

$$\tilde{g}_{\mu\nu} = g_{\mu\nu} + \frac{2}{M^2} \partial_\mu \phi \partial_\nu \phi \,, \tag{42}$$

where we are focusing solely in the non-conformal term, causes a term in the lagrangian of the type [9]

$$S = \frac{1}{M^2} \int d^4x \sqrt{-g} \partial_\mu \phi \partial_\nu \phi T^{\mu\nu} \,, \tag{43}$$

where $T^{\mu\nu}$ is the SM energy-momentum tensor built from $g_{\mu\nu}$. Recalling that for non-relativistic matter the only non-vanishing tensor element is $T^{00} = \rho$, it is easy to see that (43) is null for a static field, i.e. $\partial_0 \phi = 0$.

2.4 Axions

Among the fields produced by compactification, axions are of particular interest. These are pseudo-scalars enjoying either continuous or discrete shift symmetry

$$a \mapsto a + const. \tag{44}$$

Because of this, they can interact with the SM only through terms like $\partial_\mu a$, $\exp(ia/a_0)$ or $\cos(a/a_0)$. This has the effect of protecting their mass from UV effects. Moreover, being pseudo-scalars they evade constraints regarding spin-independent fifth-forces [10].

Closed string axions are well-suited to exemplify the previous points in more details. They arise from the integration of p-forms over p-cycles of the compact space, i.e.

$$b_I = \frac{1}{\alpha'} \int_{\Sigma_2^I} B_2 \,, \tag{45}$$

$$c_I = \frac{1}{\alpha'} \int_{\Sigma_2^I} C_2 \,, \tag{46}$$

$$\theta_I = \frac{1}{(\alpha')^2} \int_{\Sigma_4^I} C_4 \,, \tag{47}$$

where we KK-expand the 10D p-forms into 4D 0-forms as

$$B_2 = B_2(x) + b^I(x)\omega_I \,, \tag{48}$$

$$C_2 = C_2(x) + c^I(x)\omega_I \,, \tag{49}$$

$$C_4 = \theta^I(x)\tilde{\omega}_I \,. \tag{50}$$

The ω_I and $\tilde{\omega}_I$ are a basis of harmonic forms for the Dolbeault cohomology groups $H^{1,1}$ and $H^{2,2}$ respectively, normalized such that

$$\int_{\Sigma_2^I} \omega^J = \alpha' \delta_I^J \,, \tag{51}$$

$$\int_{\Sigma_4^I} \tilde{\omega}^J = (\alpha')^2 \delta_I^J \,. \tag{52}$$

For vanishing fluxes background values, the action (5) depends on the p-forms only through their field strengths. It follows that the gauge invariance of the 10D p-forms translates into a 4D axion continuous shift symmetry. This is preserved to all orders in perturbation theory, but is broken into a discrete symmetry spontaneously by non-perturbative effects in α' or g_s and explicitly by D-branes. Identifying open string axions is not as trivial. We will present a qualitative argument in Chapter 4.

2.5 Conifolds

While the compact CY_3 metrics are only known numerically, we are allowed to approximate a local region with a non-compact Calabi-Yau conifold [11][5], the metric of which is better known.

A conifold can be thought of as the locus in $\mathbb{C}_4$ defined by

$$\sum_{A=1}^{4} (z^A)^2 = 0 \,, \tag{53}$$

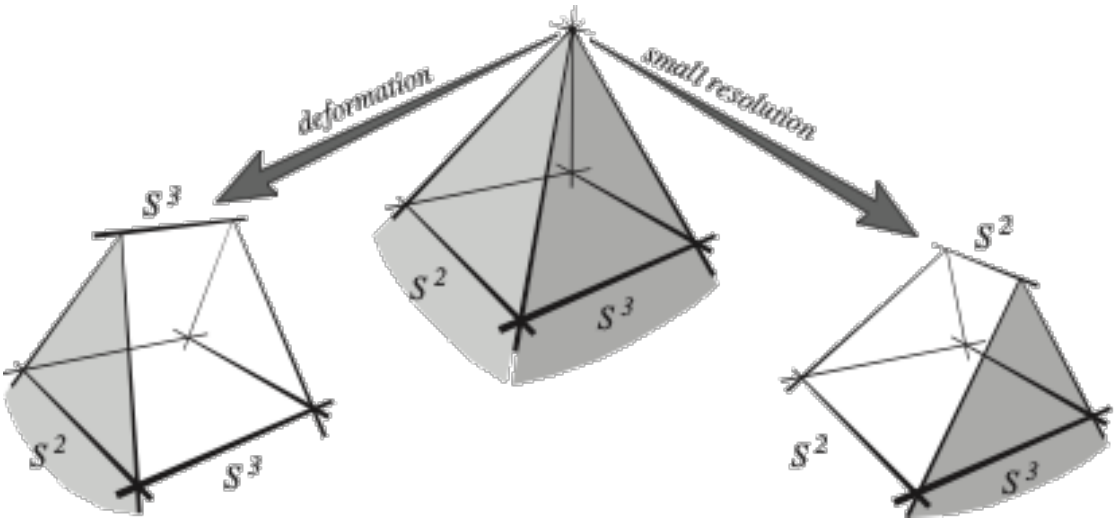

Figure 1: The singularity at the tip is avoided in the deformed and resolved conifold, where one imposes a finite minimum radius for S^3 and S^2 respectively. Figure from [12].

with z_A complex coordinates of $\mathbb{C}_4$. Alternatively, it consists of a radial direction and an Einstein manifold for base, where with this label we indicate manifolds such that $R_{ab} \propto g_{ab}$. For the 1+5-dimensional case we are interested in, the base manifold is the fibration of S^2 over S^3, or equivalently the coset space

$$T^{1,1} = [SU(2) \times SU(2)]/U(1) \tag{54}$$

with isometry group $SU(2) \times SU(2) \times U(1)$ and metric

$$d\Omega^2_{T^{1,1}} \equiv \frac{1}{9}\left(d\psi + \sum_{i=1}^{2} \cos\theta_i d\phi_i\right)^2 + \frac{1}{6}\sum_{i=1}^{2}\left(d\theta_i^2 + \sin^2\theta_i d\phi_i^2\right) \ , \tag{55}$$

where $\theta_i \in [0, \pi]$, $\phi_i \in [0, 2\pi]$ and $\psi_i \in [0, 4\pi]$. The full conifold metric can be written as

$$ds^2 = dr^2 + r^2 d\Omega^2_{T^{1,1}} \ . \tag{56}$$

From (56), one can notice that the conifold presents a singularity at $r = 0$. This corresponds to both S^2 and S^3 shrinking to a point at the tip. To avoid the singularity, it is enough to impose one of the spheres to not shrink completely. Depending on our choice, we obtain either the resolved [13] or deformed conifold [3] (see Fig. 1). In String Theory, one tends to prefer the deformed conifold, since the parameter ϵ responsible for smoothing out the tip can be interpreted as a complex structure modulus.

By adding branes on the manifold, one warps the metric. This effect is represented by the appearance of a warp factor $h(y)$ in the metric. The most well-know solution is the Klebanov-Strassler geometry [14], obtained from a deformed conifold by considering the backreaction of a stack of D3-branes at the tip and D5-branes wrapped around the collapsed S^2. Far from the tip (or equivalently for small enough ϵ), the KS metric reduces to that of a warped singular conifold [15][3]

$$ds^2 = \left(1 + \frac{L^4}{r^4}\right)^{\frac{1}{2}} \left(dr^2 + r^2 d\Omega^2_{T^{1,1}}\right), \quad L^4 = \frac{27\pi}{4} g_s N (\alpha')^2 , \tag{57}$$

where N is the number of stacked D3-branes. Apart from the numerical coefficient in L, one can appreciate the similarity to the warping induced on the simpler geometry $AdS_5 \times S^5$, often used in the context of AdS/CFT duality[1] [17][16].

In (57) the warping is sourced by a stack of D-branes at the tip. However, since the warp factor ultimately comes from the 6D Laplace equation [13][18]

$$\nabla^2 h(y) = 0 , \tag{58}$$

one can invoke the Superposition Principle for linear differential equations to generalize (58) into what is known as the multi-center solution [19][6]

$$h(y) = 1 + \frac{L_\alpha}{|\mathbf{y} - \mathbf{y}_\alpha|^4} , \tag{59}$$

representing the warping for multiple parallel and similarly-oriented branes centered at $\mathbf{y}_\alpha$.

[1] The volume modulus $\mathcal{V}$ does not appear in [16] because of a different choice of Weyl factor in (18).

3 Screening Mechanisms

When introducing new scalars on top of the SM, these often result in new interactions among matter particles, causing modifications to their equation of motion that we collect under the name of fifth-forces. However, experiments have not been able to detect these forces so far. For instance, one could hope to observe modifications to GR in the motion of macroscopical objects both on Earth and in the Solar System. The absence of such deviations causes tension between these type of beyond-SM theories and experiments.

Screening mechanisms aim to resolve this tension by introducing a matter-density dependence in the intensity of fifth-forces. More precisely, they manage to suppress fifth-forces in high-density environments, like the Solar System, while keeping them relevant on the cosmological scale.

In this chapter, we focus on (Quasi-)Brans-Dicke theories and describe the associated fifth-forces. Then we describe the working of single-field and (most importantly for us) two-field screening mechanisms.

3.1 (Quasi-)Brans-Dicke Scalars and the Equivalence Principle

BD theories (see [20] for the original paper and [21][22][23] for more recent reviews and cosmological applications) are a subclass of scalar-tensor theories. Their action was first expressed as

$$S = \frac{M_p^2}{2}\int d^4x\sqrt{-\tilde{g}}\left(\chi\tilde{R} - \frac{\omega}{\chi}\tilde{g}^{\mu\nu}\partial_\mu\chi\partial_\nu\chi\right) + S_{\mathsf{SM}}(\tilde{g}_{\mu\nu})\,, \tag{60}$$

where a non-minimal coupling is introduced between the Ricci scalar and a new scalar field.

Nowadays, we recognize this as a Jordan-frame action. To go to the Einstein frame, one introduces the Einstein metric through the Weyl rescaling

$$\tilde{g}_{\mu\nu} = \frac{1}{\chi}g_{\mu\nu}\,. \tag{61}$$

It follows that

$$\tilde{g}^{\mu\nu} = \chi g^{\mu\nu} \tag{62}$$

and

$$\sqrt{-\mathsf{det}(\tilde{g}_{\mu\nu})} = \sqrt{-\mathsf{det}\left(\frac{1}{\chi}g_{\mu\nu}\right)} = \sqrt{-\frac{1}{\chi^4}\mathsf{det}\left(g_{\mu\nu}\right)} = \frac{1}{\chi^2}\sqrt{-\mathsf{det}\left(g_{\mu\nu}\right)}\,. \tag{63}$$

The Ricci scalar is also affected by the change of metric. To see that, let us recall that for a Weyl rescaling

$$\tilde{g}_{MN} = e^{2\alpha} g_{MN} \tag{64}$$

the Ricci scalars enjoy the relation [2]

$$e^{2\alpha}\tilde{R} = R - 2(D-1)\nabla^2\alpha - (D-2)(D-1)g^{MN}\partial_M\alpha\partial_N\alpha \tag{65}$$

with ∇ evaluated from g_{MN}. To go back to our case, we just need to apply the substitutions

$$\alpha = -\frac{1}{2}\ln\chi, \quad D = 4 \tag{66}$$

and we obtain

$$\tilde{R} = \chi R + 3\chi^2\Box(\ln\chi) - \frac{3}{2}\chi g^{\mu\nu}\partial_\mu(\ln\chi)\partial_\nu(\ln\chi)\,. \tag{67}$$

The action has now become

$$\begin{aligned} S &= \frac{M_p^2}{2}\int d^4x\sqrt{-g}\left(R + 3\Box(\ln\chi) - g^{\mu\nu}\left(\frac{3}{2}\partial_\mu(\ln\chi)\partial_\nu(\ln\chi) + \frac{\omega}{\chi^2}\partial_\mu\chi\partial_\nu\chi\right)\right) + \\ &\quad + S_{\text{SM}}\left(\frac{1}{\chi}g_{\mu\nu}\right) \\ &= \frac{M_p^2}{2}\int d^4x\sqrt{-g}\left(R - \left(\frac{3}{2}+\omega\right)g^{\mu\nu}\partial_\mu(\ln\chi)\partial_\nu(\ln\chi)\right) + S_{\text{SM}}\left(\frac{1}{\chi}g_{\mu\nu}\right)\,, \end{aligned} \tag{68}$$

where in the last step we canceled the total derivative. The field redefinition

$$\phi \equiv \sqrt{\omega + \frac{3}{2}}\ln\chi \to \chi = e^{\frac{1}{\sqrt{\omega+\frac{3}{2}}}\phi} \tag{69}$$

gives us the action in canonical form

$$S = \frac{M_p^2}{2}\int d^4x\sqrt{-g}\,(R - g^{\mu\nu}\partial_\mu\phi\partial_\nu\phi) + S_{\text{SM}}\left(e^{-\frac{1}{\sqrt{\omega+\frac{3}{2}}}\phi} g_{\mu\nu}\right)\,. \tag{70}$$

Looking at this Einstein-frame action, we can interpret the BD theory as the addition of a new scalar χ with conformal coupling to matter of the form

$$\tilde{g}_{\mu\nu} = e^{2\mathfrak{g}\phi} g_{\mu\nu}\,. \tag{71}$$

As we will see, (71) has the perk of giving a constant scalar-SM coupling $\mathfrak{g}$. When generalizing to QBD theories [24], we assume a more generic Weyl factor

$$\tilde{g}_{\mu\nu} = A^2(\phi) g_{\mu\nu} \tag{72}$$

and consequently an Einstein-frame action

$$S = \frac{M_p^2}{2}\int d^4x\sqrt{-g}\,(R - \partial_\mu\phi\partial^\mu\phi) + S_{\mathsf{SM}}\left(A^2(\phi)g_{\mu\nu}\right)\ . \tag{73}$$

The reason people are interested in BD and QBD theories is because they automatically satisfy the Equivalence Principle [24]

$$\tilde{\nabla}_\nu\tilde{T}^{\mu\nu} = 0\ . \tag{74}$$

That is, the stress-energy tensor

$$\tilde{T}^{\mu\nu} = \frac{2}{\sqrt{-\tilde{g}}}\left(\frac{\delta S_{\mathsf{SM}}}{\delta\tilde{g}_{\mu\nu}}\right) \tag{75}$$

is conserved. Notice that (74) is not true for $T^{\mu\nu}$ defined through $g_{\mu\nu}$. We can prove (74) starting from the diffeomorphism invariance of S_{SM}, i.e

$$\delta_v S_{\mathsf{SM}} = \int d^4x\frac{\delta S_{\mathsf{SM}}}{\delta\tilde{g}_{\mu\nu}}\delta_v\tilde{g}_{\mu\nu} + \frac{\delta S_{\mathsf{SM}}}{\delta\Psi}\delta_v\Psi \equiv 0\ . \tag{76}$$

The second term vanishes when the SM equations of motions are satisfied. We are left with

$$\frac{\delta S_{\mathsf{SM}}}{\delta\tilde{g}_{\mu\nu}}\delta_v\tilde{g}_{\mu\nu} = \frac{\sqrt{-\tilde{g}}}{2}\tilde{T}^{\mu\nu}\left(\tilde{\nabla}_\mu v_\nu + \tilde{\nabla}_\nu v_\mu\right) = \sqrt{-g}T^{\mu\nu}\tilde{\nabla}_\mu v_\nu \equiv 0\ . \tag{77}$$

Integrating by parts gives (74).

Let us see how the scalar-SM interaction expressed through S_{SM} modifies the scalar equation of motion by applying the Variational Principle. We find

$$\begin{aligned}\frac{1}{\sqrt{-g}}\frac{\delta S_{SM}(A^2(\phi)g_{\mu\nu})}{\delta\phi} &= \frac{1}{\sqrt{-g}}\frac{\delta S_{SM}}{\delta(A^2g_{\mu\nu})}\frac{\partial(A^2g_{\mu\nu})}{\partial\phi} = \frac{1}{\sqrt{-g}}\frac{1}{A^2}\frac{\delta S_{SM}}{\delta g_{\mu\nu}}g_{\mu\nu}\frac{\partial(A^2)}{\partial\phi}\\ &= g_{\mu\nu}\frac{1}{\sqrt{-g}}\frac{1}{A^2}\frac{\delta S_{SM}}{\delta g_{\mu\nu}}2A\frac{\partial A}{\partial\phi} = g_{\mu\nu}\frac{2}{\sqrt{-g}}\frac{\delta S_{SM}}{\delta g_{\mu\nu}}\frac{1}{A}\frac{\partial A}{\partial\phi}\\ &= g_{\mu\nu}T^{\mu\nu}\partial_\phi\ln A = \partial_\phi\ln A\,T\ .\end{aligned} \tag{78}$$

That is, ϕ couples to the trace of the SM energy-momentum tensor through

$$\mathfrak{g}(\phi) = \partial_\phi\ln A\ . \tag{79}$$

Notice how for (71), this gives $\mathfrak{g} = const.$ as we claimed.

3.2 Fifth-forces from Scalar Fields

Let us now study in details how QBD theories source fifth-forces (we elaborate on the review in [25]). From (74) we know that SM-matter (approximated as dust) moves along geodesics in the Jordan frame. In the Newtonian limit, the geodesic equation is

$$\ddot{x}^i + \tilde{\Gamma}^i_{00} = \ddot{x}^i + \Gamma^i_{00} + \mathfrak{g}(\phi)\partial^i\phi = 0 \,, \tag{80}$$

where $\tilde{\Gamma}^i_{00}$ and Γ^i_{00} are Christoffel symbols of the Jordan and Einstein metric respectively related through (72). The same way one interprets Γ^i_{00} as the Newtonian force,

$$F_5 \equiv -\mathfrak{g}(\phi)\nabla\phi \tag{81}$$

represents a new fifth-force[2].

We have already shown in (78) how interaction with the SM results in an additional term in the scalar equation of motion. In general, one has something like

$$\Box(\phi) = \frac{1}{M_p^2}\frac{\mathsf{d}V(\phi)}{\mathsf{d}\phi} + \frac{1}{M_p^2}\mathfrak{g}(\phi)\rho = \frac{1}{M_p^2}\frac{\mathsf{d}V_{\mathsf{eff}}(\phi)}{\mathsf{d}\phi} \,, \tag{82}$$

where we defined the effective potential

$$V_{\mathsf{eff}}(\phi) \equiv V(\phi) + \rho \mathsf{ln} A(\phi) \,. \tag{83}$$

As usual, one finds the field mass through

$$m^2_{\mathsf{eff}}(\phi) = \frac{1}{M_p^2}V''_{\mathsf{eff}}(\phi) \,. \tag{84}$$

Notice how both the coupling $\mathfrak{g}$ and the mass m_{eff} are functions of the field ϕ. To fix these, one imagines the field to be around a minimum of V_{eff}, in order to perform a background-perturbation split

$$\phi = \phi_0 + \delta\phi \,, \tag{85}$$

where ϕ_0 is the field evaluated at the minimum. For now we assume, as most research does, ϕ_0 to be spatially uniform (although this is not going to be the case for our model in Chapter 4). Close to its minimum, we can approximate the effective potential to

$$V(\phi) \simeq \frac{M_p^2}{2}m^2_{\mathsf{eff}}(\phi_0)(\delta\phi)^2 \,. \tag{86}$$

[2]Notice that F_5 is missing the mass of the moving particle to be an actual force, so it has the mass dimension of an acceleration, i.e 1. For this same reason, when we later write $F_5(r) = -\partial_r V(r)$, we use V as a potential and not as the potential energy density as we do in the rest of the thesis.

Finally, we obtain from (82) the static equation of motion with a source for a massive scalar

$$\left(\nabla^2 - m_{\text{eff}}^2(\phi_0)\right)\delta\phi = \frac{1}{M_p^2}\mathfrak{g}(\phi_0)\rho(r)\,, \tag{87}$$

which is solved by

$$\delta\phi = -\frac{1}{M_p^2}\frac{\mathfrak{g}(\phi_0)}{4\pi}\frac{f(M,R)}{r}e^{-m_{\text{eff}}r} \tag{88}$$

if we assume the source to be spherically symmetric. Here $f(M,R)$ is a function of the source mass and radius. Notice that we expect it to have mass dimension 1. From now on, we drop the delta in $\delta\phi$ to lighten the notation.

Let us obtain (88) explicitly, momentarily sending m_{eff} into m again for ease of readability. We start from the Fourier expansions of the field and the source density

$$\phi(\mathbf{x}) = \frac{1}{(2\pi)^3}\int d^3k e^{i\mathbf{k}\cdot\mathbf{x}}\tilde{\phi}(\mathbf{k})\,, \tag{89}$$

$$\rho(r) = \frac{1}{(2\pi)^3}\int d^3k e^{i\mathbf{k}\cdot\mathbf{x}}\tilde{\rho}(k)\,. \tag{90}$$

Since $\rho(r)$ has spherical symmetry, we can express its Fourier transform as [26]

$$\tilde{\rho}(k) = (2\pi)^{\frac{n}{2}}k^{\frac{2-n}{2}}\int_0^{+\infty} dr r^{\frac{n}{2}}\rho(r)J_{\frac{n-2}{2}}(kr)\,, \tag{91}$$

where we are using the first order ordinary Bessel functions [26]

$$J_m(x) = \left(\frac{x}{2}\right)^m\sum_{l=0}^{+\infty}\frac{(-1)^l\left(\frac{x}{2}\right)^{2l}}{l!\Gamma(m+l+1)}\,. \tag{92}$$

For us the number of dimensions $n = 3$, so it is relevant to point out the special result

$$J_{\frac{1}{2}}(x) = \sqrt{\frac{2}{\pi x}}\sin x\,. \tag{93}$$

Using (93), we simplify (91) into

$$\tilde{\rho}(k) = 4\pi\int_0^{+\infty} dr r^2\frac{\sin(kr)}{kr}\rho(r)\,, \tag{94}$$

from which it is easy to see that $\tilde{\rho}$ dependent just on the modulus k, is even and has no poles. Although it seems like (94) could give problems regarding convergence, these are avoided if one considers a finite-size source, i.e $\rho(r) = 0$ for $r > R$. It is instructive (and a good quality check) to consider the point-source case, i.e

$$\rho(r) = M\delta^3(\mathbf{x}) = M\frac{\delta(r)}{4\pi r^2}, \quad \mathbf{x}, r = 0\,, \tag{95}$$

where we used

$$\begin{aligned}\int d^3x\delta^3(\mathbf{x}) &= \int_0^{+\infty} drr^2 \int_0^{\pi} d\theta \sin\theta \int_0^{2\pi} d\varphi\delta^3(\mathbf{x}) \\ &= \int_0^{+\infty} dr 4\pi r^2\delta^3(\mathbf{x}) \equiv \int_0^{+\infty} dr\delta(r)\,,\end{aligned} \tag{96}$$

which implies

$$\delta^3(\mathbf{x}) = \frac{\delta(r)}{4\pi r^2}\,. \tag{97}$$

Plugging (95) into (94) results in $\tilde{\rho} = M$. We can finally apply (89) and (90) to (87) to obtain the momentum-space equation of motion

$$-(k^2+m^2)\tilde{\phi}(\mathbf{k}) = \frac{1}{M_p^2}\mathfrak{g}\tilde{\rho}(k)\,. \tag{98}$$

Isolating $\tilde{\phi}$ gives us the propagator

$$\tilde{\phi}(\mathbf{k}) = -\frac{1}{M_p^2}\frac{\mathfrak{g}\tilde{\rho}(k)}{k^2+m^2}\,. \tag{99}$$

From here, all that is left to do is evaluate (89), resulting in

$$\begin{aligned}\phi(r) &= -\frac{1}{M_p^2}\frac{\mathfrak{g}}{(2\pi)^3}\int d^3k e^{i\mathbf{k}\cdot\mathbf{x}}\frac{\tilde{\rho}(k)}{k^2+m^2} \\ &= -\frac{1}{M_p^2}\frac{\mathfrak{g}}{(2\pi)^3}\int_0^{+\infty} dkk^2\int_0^{\pi} d\theta\sin\theta\int_0^{2\pi} d\varphi e^{ikr\cos\theta}\frac{\tilde{\rho}(k)}{k^2+m^2} \\ &= -\frac{1}{M_p^2}\frac{\mathfrak{g}}{(2\pi)^2}\int_0^{+\infty} dkk^2\frac{\tilde{\rho}(k)}{k^2+m^2}\int_{-1}^{1} d(\cos\theta)e^{ikr\cos\theta} \\ &= -\frac{1}{M_p^2}\frac{\mathfrak{g}}{(2\pi)^2}\int_0^{+\infty} dkk^2\frac{\tilde{\rho}(k)}{k^2+m^2}\frac{1}{ikr}\left(e^{ikr}-e^{-ikr}\right) \\ &= -\frac{1}{M_p^2}\frac{\mathfrak{g}}{(2\pi)^2 ir}\int_{-\infty}^{+\infty} dkk\frac{\tilde{\rho}(k)}{k^2+m^2}e^{ikr} \\ &= -\frac{1}{M_p^2}\frac{\mathfrak{g}}{(2\pi)^2 ir}2\pi i\,\mathrm{Res}\left[\frac{k\tilde{\rho}(k)}{k^2+m^2}e^{ikr}\right]_{k=im} \\ &= -\frac{1}{M_p^2}\frac{\mathfrak{g}}{4\pi}\frac{\tilde{\rho}(im)e^{-mr}}{r}\end{aligned} \tag{100}$$

as we claimed. Notice that from (94)

$$\begin{aligned}\tilde{\rho}(im) &= 4\pi\int_0^{+\infty} drr^2\frac{e^{i(im)r}-e^{-i(im)r}}{2i(im)r}\rho(r) = 4\pi\int_0^{+\infty} drr^2\frac{e^{mr}-e^{-mr}}{2mr}\rho(r) \\ &= 4\pi\int_0^{+\infty} drr^2\frac{\sinh(mr)}{mr}\rho(r)\in\mathbb{R}\,.\end{aligned} \tag{101}$$

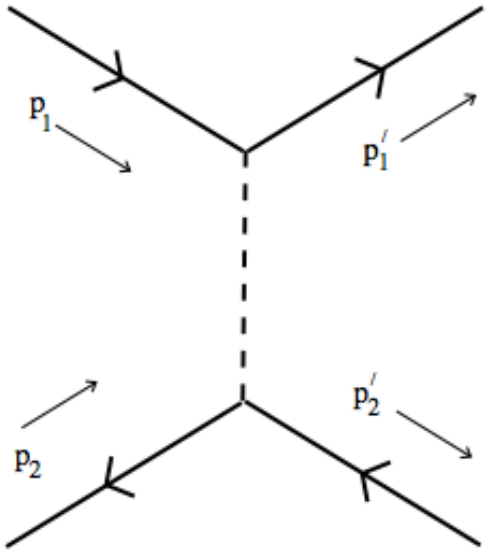

Figure 2: Feynman diagram of a scalar exchange t-channel.

Now that we have proven (88), we can use it in (81) to find

$$F_5(r) = -\mathfrak{g}(\phi_0)\partial_r\phi = -\frac{1}{M_p^2}\frac{\mathfrak{g}^2(\phi_0)f(M,R)e^{-m_{\text{eff}}(\phi_0)r}}{4\pi r^2}(1+m_{\text{eff}}(\phi_0)r)\,. \tag{102}$$

To find the associated potential, we use

$$F_5(r) = -\partial_r V(r)\,, \tag{103}$$

which gives [27]

$$V(r) = \mathfrak{g}(\phi_0)\phi(r) = -\frac{1}{M_p^2}\frac{\mathfrak{g}^2(\phi_0)}{4\pi}\frac{f(M,R)e^{-m_{\text{eff}}(\phi_0)r}}{r}\,. \tag{104}$$

From a QFT perspective, we recognize in (87) and (99) the Klein-Gordon equation and propagator respectively, if we assumed a point-source, i.e. $\tilde{\rho} = M$. Indeed, in this case (104) would be the standard Yukawa potential one obtains integrating over **k** the tree-level amplitude of and interaction like

$$L_{\text{int}} = \mathfrak{g}\bar{\psi}\phi\psi\,, \tag{105}$$

representing a scalar exchange between matter particles (see Fig. 2).

3.3 Single-field Screening Mechanisms

Looking at (102), one can think of at least two ways to reduce F_5 in the Solar System without relying on fine-tuning: $m_{\text{eff}} \gg 1$ or $\mathfrak{g} \ll 1$. This is possible thanks to these parameters' dependence on the minimum ϕ_0. The two strategies above represent examples of single-field screening mechanisms: the chameleon and symmetron screening mechanism respectively. Let us see how these work in details.

3.3.1 Chameleon Screening

The chameleon screening mechanism achieves high m_{eff} in regions of high density ρ and low m_{eff} in regions of low ρ. This is possible for specific choices of potential $V(\phi)$ and Weyl factors $A(\phi)$. Here we illustrate the mechanism with [25]

$$V(\phi) = \frac{\Lambda^{n+4}}{M_p^n \phi^n} \,, \tag{106}$$

where Λ is just a scale factor with mass dimension 1, and [25]

$$A(\phi) = e^{\mathfrak{g}\phi} \,, \tag{107}$$

which using (83) gives

$$V_{\text{eff}}(\phi) = \frac{\Lambda^{n+4}}{M_p^n \phi^n} + \rho \mathfrak{g} \phi \,. \tag{108}$$

A ρ-dependent minimum exists for $n = -2, -4, -6, ...$ and $n \geq 1$ and it is

$$\phi_0(\rho) = \left(\frac{n\Lambda^{n+4}}{M_p^n \mathfrak{g} \rho} \right)^{\frac{1}{n+1}} \,. \tag{109}$$

The effective mass is given by

$$m_{\text{eff}}^2(\rho) = \frac{1}{M_p^2} V''_{\text{eff}}(\phi_0) = \frac{n(n+1)}{M_p^{n+2}} \Lambda^{n+4} \left(\frac{M_p^n \mathfrak{g} \rho}{n\Lambda^{n+4}} \right)^{\frac{n+2}{n+1}} \,. \tag{110}$$

Notice that for $n = -2$ (110) loses the dependence on ρ. By plotting (108) in Fig. 3, one can see from the width of the valley that m_{eff} grows with ρ as we aimed.

3.3.2 Symmetron Screening

The symmetron screening mechanism uses density-induced symmetry restoration. We start from a potential [25]

$$\frac{V(\phi)}{M_p^4} = -\frac{1}{2}\mu^2 \phi^2 + \frac{\lambda}{4}\phi^4 \tag{111}$$

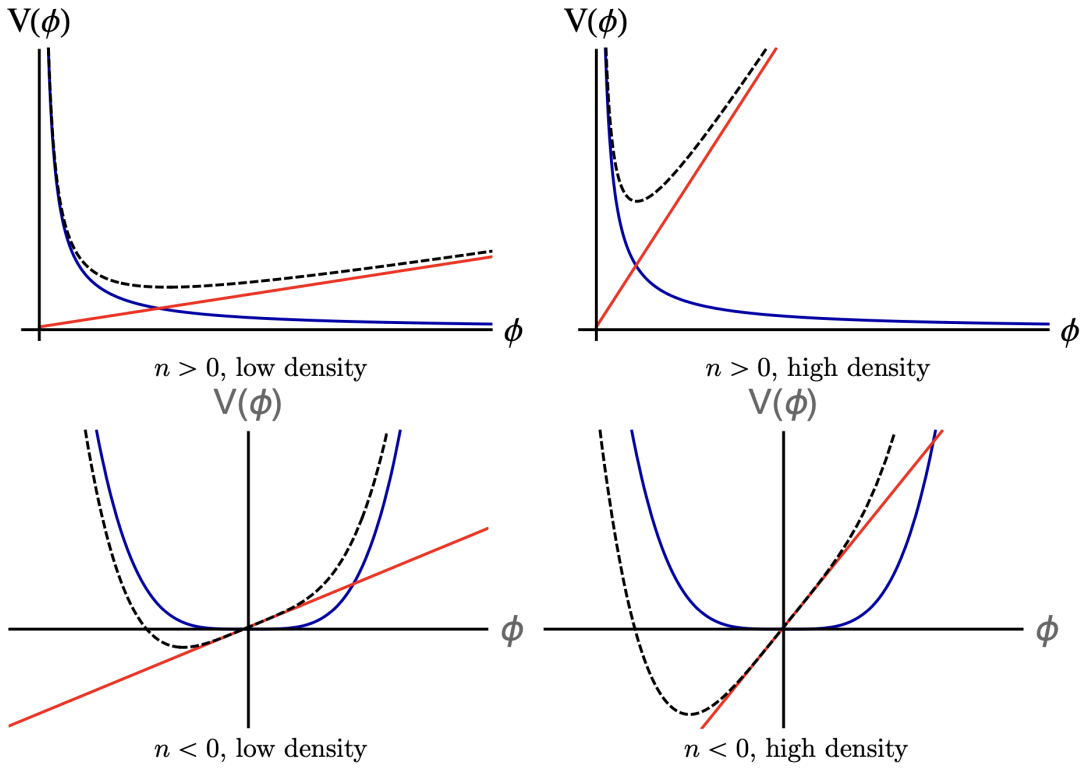

Figure 3: Sketches of the chameleon effective potential for positive n (upper panels) and negative n (lower panels). The left and right panels show the cases of low and high density environments respectively. The blue lines show the bare potential and the red lines show the contribution from the coupling to matter. The black dashed lines show the resultant effective potential, which is the sum of the red and blue lines, and governs the dynamics of the scalar. Figure from [25].

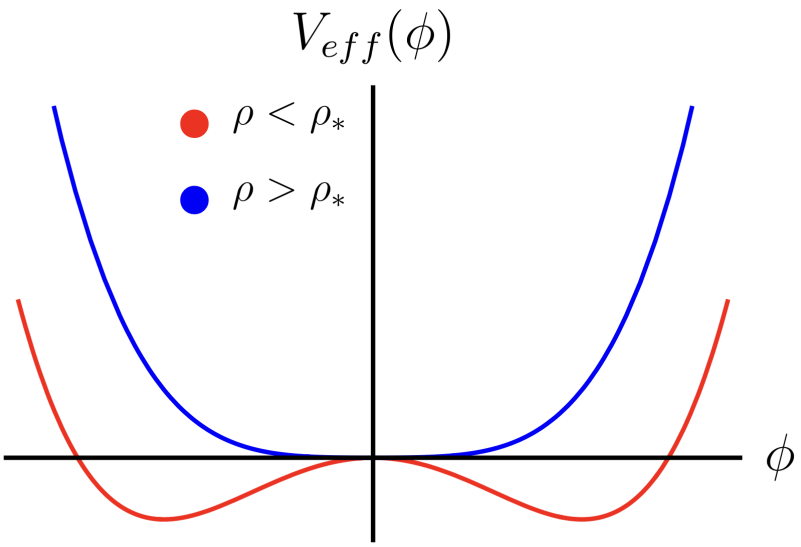

Figure 4: The effective potential for the symmetron when $\rho < \rho_\star$ (red) and when $\rho > \rho_\star$ (blue). Figure from [25].

with $\lambda > 0$, and the Weyl factor [25]

$$A(\phi) = 1 + \frac{\phi^2}{2k_s^2} \tag{112}$$

with k_s a numerical factor. Combined, these give an effective potential

$$\frac{V_{\text{eff}}(\phi)}{M_p^4} = -\frac{1}{2}\mu^2\phi^2 + \frac{\lambda}{4}\phi^4 + \frac{\rho}{M_p^4}\ln\left(1 + \frac{\phi^2}{2k_s^2}\right) \simeq -\frac{1}{2}\mu^2\left(1 - \frac{\rho}{M_p^4\mu^2k_s^2}\right)\phi^2 + \frac{\lambda}{4}\phi^4 \tag{113}$$

for small ϕ. The value

$$\rho_\star \equiv M_p^4\mu^2M_s^2 \tag{114}$$

plays the role of a critical density. For $\rho < \rho_\star$ the quadratic term in (113) has negative coefficient, while it is positive for $\rho > \rho_\star$. The two cases correspond to broken and restored $\mathbb{Z}_2$ symmetry. When symmetry is broken, we find two minima

$$\phi_0^\pm = \pm\frac{\mu}{\sqrt{\lambda}}\sqrt{1 - \frac{\rho}{\rho_\star}} \xrightarrow{\rho \ll \rho_\star} \pm\frac{\mu}{\sqrt{\lambda}} \tag{115}$$

and, using (79),

$$\mathfrak{g}(\phi_0) \simeq \left|\frac{\phi_0^\pm}{k_s^2}\right| \simeq \frac{\mu}{\sqrt{\lambda}k_s^2}\,. \tag{116}$$

If the symmetry is restored, $\phi_0 = 0$ and $\mathfrak{g} = 0$. Basically, this mechanism turns off coupling to the SM in regions of density greater than a certain threshold (see Fig. 4).

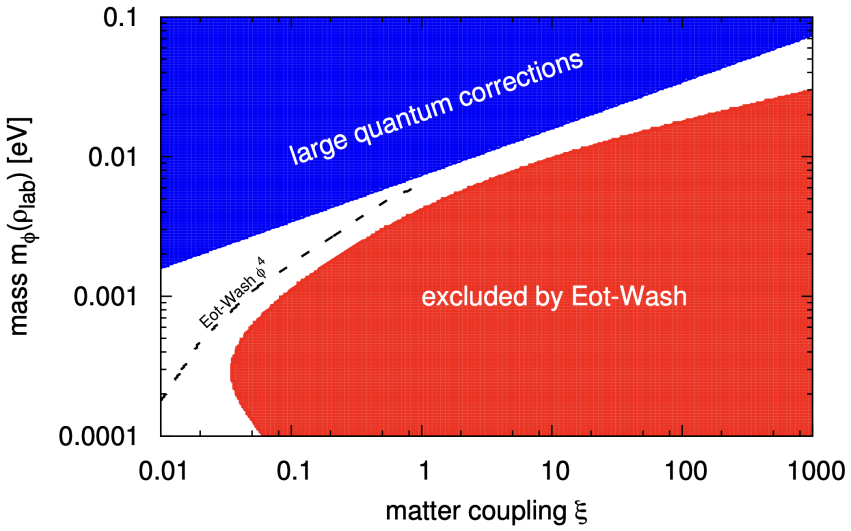

Figure 5: Model-independent constraints on chameleon fields in the $\mathfrak{g}$, m_{eff} plane with $\rho_{\text{lab}} = 10\text{g/cm}^3$. Shaded regions show loop bounds from (125) and experimental constraints from Eöt-Wash [28]. The dashed curve shows the direct bound on the ϕ^4 model for $\mathfrak{g} < 1$ [29], converted to m_{eff}. Figure from [30].

3.3.3 Instability due to Quantum Corrections

As we have seen above for some examples, single-field screening mechanisms rely heavily on specific shapes for the potential. However, quantum effects can spoil these through Coleman-Weinberg corrections [31], nullifying the screening mechanism one had achieved classically. In particular, here we focus on the instability these corrections bring to the chameleon screening mechanism [30].

Coleman-Weinberg corrections grow more and more relevant as the mass of the scalar field increases. This causes some tension, since in high-density regions ϕ should be heavy enough to achieve significant screening, but also light enough to suppress quantum correction to the potential. As a result, m_{eff} ends up squeezed in a quite narrow region (see Fig. 5).

Let us be more quantitative. For scalar fields, 1-loop Coleman-Weinberg corrections are given by [31]

$$\Delta V_{\text{1-loop}}(\phi) = \frac{m_{\text{eff}}^4(\phi)}{64\pi^2} \ln\left(\frac{m_{\text{eff}}^2(\phi)}{\mu_0^2}\right) \tag{117}$$

with μ_0 arbitrary mass scale. Since we are interested in scalars with low mass but high m_{eff}, we assume most of the potential contribution to come from SM interaction, meaning

$$V_{\text{eff}}(\phi) \simeq \mathfrak{g}\rho\phi\,. \tag{118}$$

For the classical theory to be predictive, we need quantum corrections not to change the potential minimum ϕ_0 and the effective mass m_{eff} too much. Since the first is related to V'_{eff} and the second to V''_{eff}, this means requiring

$$\left|\frac{\Delta V'_{\text{1-loop}}}{V'_{\text{eff}}}\right| \simeq \left|\frac{(m^4_{\text{eff}})'}{64\pi^2\mathfrak{g}\rho}\right| < \epsilon \,, \tag{119}$$

$$\left|\frac{\Delta V''_{\text{1-loop}}}{V''_{\text{eff}}}\right| \simeq \left|\frac{(m^4_{\text{eff}})''}{64\pi^2 m^2_{\text{eff}}}\right| < \epsilon \,, \tag{120}$$

where all primes represent derivation with respect to ϕ and we approximated (117) by setting the logarithm to unity [30].

We can go from ∂_ϕ to ∂_ρ by noticing that

$$\frac{\partial^2 V_{\text{eff}}}{\partial\rho\partial\phi} = \mathfrak{g} = \frac{\partial^2 V_{\text{eff}}}{\partial^2\phi}\frac{\partial\phi}{\partial\rho} = M_p^2 m^2_{\text{eff}}\frac{\partial\phi}{\partial\rho} \to \frac{\partial\phi}{\partial\rho} = \frac{\mathfrak{g}}{M_p^2 m^2_{\text{eff}}} \,. \tag{121}$$

This, together with

$$\frac{\partial(m^6)}{\partial\rho} = \frac{\partial(m^6)}{\partial(m^4)}\frac{\partial(m^4)}{\partial\rho} = \frac{3}{2}m^2\frac{\partial(m^4)}{\partial\rho} \tag{122}$$

and

$$\begin{aligned}\frac{\partial^2(m^6)}{\partial\rho^2} &= \frac{3}{2}\frac{\partial}{\partial\rho}\left(m^2\frac{\partial(m^4)}{\partial\rho}\right) = \frac{3}{2}\left(m^2\frac{\partial^2(m^4)}{\partial\rho^2} + \frac{1}{2m^2}\frac{\partial(m^4)}{\partial\rho}\right) \\ &\xrightarrow{m_{\text{eff}}\gg 1} \frac{3}{2}m^2\frac{\partial^2(m^4)}{\partial\rho^2} \,,\end{aligned} \tag{123}$$

turns (119) and (120) into

$$\frac{1}{\rho}\frac{\mathrm{d}m^6_{\text{eff}}}{\mathrm{d}\rho}, \left|\frac{\mathrm{d}^2 m^6_{\text{eff}}}{\mathrm{d}\rho^2}\right| \leq 96\pi^2\mathfrak{g}^2\epsilon \,. \tag{124}$$

Integrating, we find [30]

$$m_{\text{eff}} \leq \left(48\pi^2\mathfrak{g}^2\rho^2_{\text{lab}}\epsilon\right)^{\frac{1}{6}} \simeq 0.0073\left(\frac{\mathfrak{g}\rho_{\text{lab}}}{10\text{gcm}^{-3}}\right)^{\frac{1}{3}}\epsilon^{\frac{1}{6}}\text{eV} \,. \tag{125}$$

By setting $\epsilon = 1$ and $\rho_{\text{lab}} = 10\text{g/cm}^3$, we get our constraint on the effective mass and coupling constant. Combining them with experimental constraints on fifth-forces, bounding m_{eff} from below, we get Fig. 5.

3.4 The Axio-Chameleon Screening Mechanism

The axio-chameleon screening mechanism presented in [1] has its novelty in the introduction of a second scalar field: an axion a. The backbone of the mechanism is no longer the scalar potential, but a generalized kinetic term

$$L \supset -\sqrt{-g}\frac{f^2}{2}\mathcal{G}_{ab}(\phi)\partial_\mu\phi^a\partial^\mu\phi^b \,. \tag{126}$$

Because axio-chameleon screening does not rely on properties of the scalar potential, it is robust against the quantum corrections that endanger single-field screening, discussed in section 3.3.3.

The non-linear sigma model (126) together with the Einstein-Hilbert term give the action

$$S = \int d^4x\sqrt{-g_4}\left(\frac{M_p^2}{2}R_4 - \frac{f^2}{2}\mathcal{G}_{ab}(\phi)\partial_\mu\phi^a\partial^\mu\phi^b - V(\phi)\right) \,, \tag{127}$$

from which the Variational Principle provides the equation of motion

$$\frac{1}{\sqrt{-g}}\partial_\mu\left(\sqrt{-g}\mathcal{G}_{cb}\partial^\mu\phi^b\right) - \frac{1}{2}\partial_c\mathcal{G}_{ab}\partial_\mu\phi^a\partial^\mu\phi^b - \frac{\partial_c V}{f^2} = 0 \,. \tag{128}$$

Let us see how in details. We start by evaluating

$$-\frac{1}{f^2}\frac{\delta S}{\delta\phi^c} = \sqrt{-g}\frac{1}{2}\frac{\partial}{\partial\phi^c}(\mathcal{G}_{ab}\partial_\mu\phi^a\partial^\mu\phi^b) + \sqrt{-g}\frac{\partial_c V}{f^2} \,, \tag{129}$$

where the first term can be expanded into

$$\begin{aligned}\frac{\partial}{\partial\phi^c}(\mathcal{G}_{ab}\partial_\mu\phi^a\partial^\mu\phi^b) &= \partial_c\mathcal{G}_{ab}\partial_\mu\phi^a\partial^\mu\phi^b + \mathcal{G}_{ab}\partial_c(\partial_\mu\phi^a\partial^\mu\phi^b) \\ &= \partial_c\mathcal{G}_{ab}\partial_\mu\phi^a\partial^\mu\phi^b + \mathcal{G}_{ab}(\partial_\mu\partial_c\phi^a\partial^\mu\phi^b + \partial_\mu\phi^a\partial^\mu\partial_c\phi^b) \\ &= \partial_c\mathcal{G}_{ab}\partial_\mu\phi^a\partial^\mu\phi^b + \mathcal{G}_{ab}(\partial_\mu\delta^a_c\partial^\mu\phi^b + \partial_\mu\phi^a\partial^\mu\delta^b_c) \,,\end{aligned} \tag{130}$$

turning (129) into

$$-\frac{1}{f^2}\frac{\delta S}{\delta\phi^c} = \sqrt{-g}\frac{1}{2}\partial_c\mathcal{G}_{ab}\partial_\mu\phi^a\partial^\mu\phi^b + \sqrt{-g}\frac{1}{2}\mathcal{G}_{ab}(\partial_\mu\delta^a_c\partial^\mu\phi^b + \partial_\mu\phi^a\partial^\mu\delta^b_c) + \sqrt{-g}\frac{\partial_c V}{f^2} \,. \tag{131}$$

Here, the second term can be integrated by parts, obtaining

$$\begin{aligned}&\sqrt{-g}\frac{1}{2}\mathcal{G}_{ab}(\partial_\mu\delta^a_c\partial^\mu\phi^b + \partial_\mu\phi^a\partial^\mu\delta^b_c) \\ &\qquad = -\partial_\mu\left(\sqrt{-g}\frac{1}{2}\mathcal{G}_{ab}\partial^\mu\phi^b\right)\delta^a_c - \partial^\mu\left(\sqrt{-g}\frac{1}{2}\mathcal{G}_{ab}\partial_\mu\phi^a\right)\delta^b_c \\ &\qquad = -\partial_\mu\left(\sqrt{-g}\mathcal{G}_{cb}\partial^\mu\phi^b\right) \,.\end{aligned} \tag{132}$$

We find (128) by imposing

$$\frac{1}{\sqrt{-g}f^2}\frac{\delta S}{\delta\phi^c} = 0\,. \tag{133}$$

The equation of motion can equivalently be expressed as

$$\mathcal{G}_{cb}\left(\Box\phi^b + \Gamma^b_{ad}\partial_\mu\phi^a\partial^\mu\phi^b\right) - \frac{\partial_c V}{f^2} = 0\,, \tag{134}$$

as one can see by making the following considerations. Firstly,

$$\begin{aligned}\frac{1}{\sqrt{-g}}\partial_\mu\left(\sqrt{-g}\mathcal{G}_{cb}\partial^\mu\phi^b\right) &= \frac{1}{\sqrt{-g}}\sqrt{-g}\mathcal{G}_{cb}\partial_\mu\partial^\mu\phi^b + \frac{1}{\sqrt{-g}}\partial_\mu\left(\sqrt{-g}\mathcal{G}_{cb}\right)\partial^\mu\phi^b \\ &= \mathcal{G}_{cb}\partial_\mu\partial^\mu\phi^b + \frac{1}{\sqrt{-g}}\partial_\mu\sqrt{-g}\mathcal{G}_{cb}\partial^\mu\phi^b + \partial_\mu\mathcal{G}_{cb}\partial^\mu\phi^b\,.\end{aligned} \tag{135}$$

Secondly,

$$\partial_\mu\mathcal{G}_{cb}\partial^\mu\phi^b = \frac{\partial\mathcal{G}_{cb}}{\partial\phi^d}\partial_\mu\phi^d\partial^\mu\phi^b = \frac{1}{2}\left(\partial_d\mathcal{G}_{cb} + \partial_b\mathcal{G}_{cd}\right)\partial_\mu\phi^b\partial^\mu\phi^d\,, \tag{136}$$

where we used the symmetry of the term under $b \leftrightarrow d$ swap. Together, these two insights allow us to rewrite (128) as

$$\begin{aligned}&\left[\mathcal{G}_{cb}\partial_\mu\partial^\mu\phi^b + \frac{1}{\sqrt{-g}}\partial_\mu\sqrt{-g}\mathcal{G}_{cb}\partial^\mu\phi^b\right] + \\ &+\left[\frac{1}{2}\left(\partial_d\mathcal{G}_{cb} + \partial_b\mathcal{G}_{cd}\right)\partial_\mu\phi^b\partial^\mu\phi^d - \frac{1}{2}\partial_c\mathcal{G}_{ab}\partial_\mu\phi^a\partial^\mu\phi^b\right] - \frac{\partial_c V}{f^2} = 0\,.\end{aligned} \tag{137}$$

The first bracket can be simplified into

$$\mathcal{G}_{cb}\frac{1}{\sqrt{-g}}\left(\sqrt{-g}\partial_\mu\partial^\mu\phi^b + \partial_\mu\sqrt{-g}\partial^\mu\phi^b\right) = \mathcal{G}_{cb}\frac{1}{\sqrt{-g}}\partial_\mu\left(\sqrt{-g}\partial^\mu\phi^b\right) = \mathcal{G}_{cb}\Box\phi^b \tag{138}$$

using

$$\frac{1}{\sqrt{-g}}\partial_\mu\left(\sqrt{-g}\partial^\mu\phi\right) = \Box\phi\,, \tag{139}$$

while the second into

$$\begin{aligned}&\frac{1}{2}\left(\partial_d\mathcal{G}_{cb} + \partial_b\mathcal{G}_{cd} - \partial_c\mathcal{G}_{bd}\right)\partial_\mu\phi^b\partial^\mu\phi^d \\ &= \mathcal{G}_{ac}\mathcal{G}^{ac}\frac{1}{2}\left(\partial_d\mathcal{G}_{cb} + \partial_b\mathcal{G}_{cd} - \partial_c\mathcal{G}_{bd}\right)\partial_\mu\phi^b\partial^\mu\phi^d \\ &= \mathcal{G}_{ac}\Gamma^a_{bd}\partial_\mu\phi^b\partial^\mu\phi^d\,,\end{aligned} \tag{140}$$

giving us precisely (134).

As we anticipated, two fields are considered in this model: the saxion-axion pair $\{\phi^1, \phi^2\} \equiv \{\phi, a\}$. By virtue of the axion shift-symmetry, the target-space metric $\mathcal{G}_{ab}$ must be independent of a. Without loss of generality, one can write [32]

$$\mathcal{G}_{ab} = \begin{pmatrix} \frac{M_p^2}{f^2} & 0 \\ 0 & W^2(\phi) \end{pmatrix} , \tag{141}$$

where the overall scale factor has been chosen such to put ϕ in canonical form in (127). Direct calculations reveal that the only non-vanishing Christoffel symbols are

$$\Gamma^1_{22} = -\frac{f^2}{M_p^2} W W' , \tag{142}$$

$$\Gamma^2_{12} = \Gamma^2_{21} = \frac{W'}{W} , \tag{143}$$

where primes represent derivation with respect to ϕ. Also, since we are interested in screening a light saxion, we assume ϕ to be a flat direction in the scalar potential, i.e. $V = V(a)$. As was the case for single-field screening mechanism, we introduce a saxion-SM interaction of the QBD type in order to preserve the Equivalence Principle. This addition, (273), (142) and (143) turn (127) into

$$S = \int d^4x \sqrt{-g_4} \left(\frac{M_p^2}{2} R_4 - \frac{M_p^2}{2} \partial_\mu \phi \partial^\mu \phi - \frac{1}{2} f^2 W^2 \partial_\mu a \partial^\mu a - V(a) \right) + S_{\mathsf{SM}}(\tilde{g}_{\mu\nu}) \tag{144}$$

and the equation of motion into

$$\Box \phi - \frac{f^2}{M_p^2} W W' (\partial a)^2 + \frac{\mathfrak{g} T}{M_p^2} = 0 , \tag{145}$$

$$\nabla_\mu (W^2 \partial^\mu a) - \frac{\partial_a V + \partial_a U}{f^2} = 0 , \tag{146}$$

where in (145) one can recognize the QBD source term coming from (78), while in (146)

$$\partial_a U \equiv -\frac{1}{\sqrt{-g}} \frac{\delta S_{\mathsf{SM}}}{\delta a} \tag{147}$$

represents direct axion-SM interaction [1].

For non-relativistic matter $T \simeq -\rho$, so (145) becomes

$$\Box \phi - \frac{f^2}{M_p^2} W W' (\partial a)^2 - \frac{\mathfrak{g} \rho}{M_p^2} = 0 . \tag{148}$$

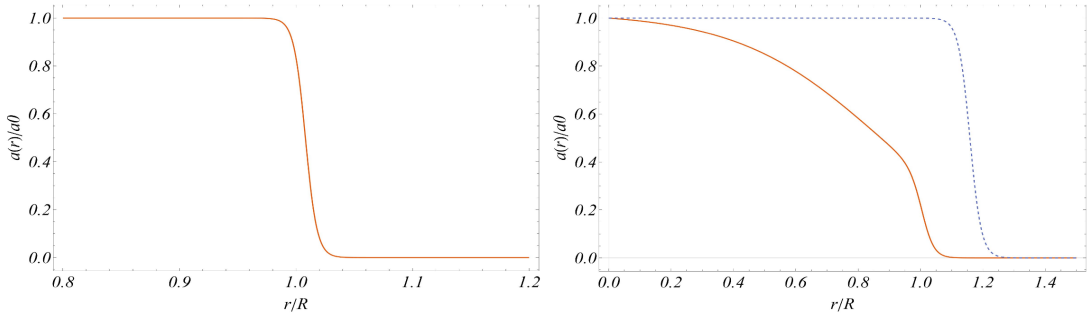

Figure 6: Calculated axion profile $a(r)$ as a function of the radius in the adiabatic approximation [1]. The external minimum is chosen to be $a_+ = 0$. The left panel uses a step-function matter-density profile and the right panel a decaying exponential profile. The solid and dashed lines in the right panel differ only in the value used for the eternal axion mass, with the solid line using a larger value. Figure from [1].

Since we are assuming a static, spherically symmetric system, we can use $\Box = \nabla^2 = \partial_r(r^2\partial_r)/r^2$ to find the equation of motion in the radial coordinate

$$M_p^2 \left(r^2\phi'\right)' = r^2 \mathfrak{g}\rho + f^2 r^2 W W'(a')^2 \,, \tag{149}$$

where primes on ϕ and a indicate derivation with respect to r.

In (149) one can recognize the kinetic term, the matter source term and the saxion-axion interaction term arising from the non-linear sigma model. In particular, notice how this last one is related to the axion gradient. Different terms are going to be relevant or not in different environments. By simplifying the matter distribution of the solar system with just the Sun itself (as we must given our assumption of spherical symmetry), we can define three regions: outside the Sun ($r > R$), inside ($r < R - l$) and close to the surface ($R - l < r < R$ with $l \ll R$).

We isolate the third region on its own because we know most of the axion gradient to be concentrated here, the reason being the following. One expects axion-matter coupling inside the Sun to contribute to the effective axion potential, giving something like

$$V_{\text{eff}}(a) = V(a) + U(a)F(r) = \frac{1}{2}m_{\text{out}}^2 f^2 (a - a_+)^2 + \frac{1}{2}m_{\text{in}}^2 f^2 (a - a_-)^2 F(r) \,, \tag{150}$$

where $F(r)$ is a normalized function proportional to the density of matter coupled to a. Assuming $m_{\text{out}} \ll m_{\text{in}}$, a_- and a_+ are the field minima inside and outside the Sun respectively and the gradient between the two happens in a narrow layer just beneath the surface of the Sun [1] (see Fig. 6).

We can finally give our full attention to (149). For $r > R$, $\rho = 0$ and $a = a_+$, therefore (149) simplifies to

$$\left(r^2 \phi'_{\text{ext}}\right)' = 0 \,, \tag{151}$$

which is solved by

$$\phi_{\text{ext}} = \phi_\infty - \frac{L}{r} \,, \tag{152}$$

where ϕ_∞ is the asymptote at infinity and we introduced

$$L \equiv (r^2 \phi')_{r=R} = r^2 \phi'_{\text{ext}} \,. \tag{153}$$

Combining (81) with (153), one can notice that $F_5 \propto \phi'_{\text{ext}} \propto L$. Our goal of screening fifth-forces can then be reformulated in terms of L. In particular, we want our mechanism to drive L to small values.

Through integration, (149) can be also expressed as

$$\phi'(r) = \frac{1}{M_p^2 r^2} \int_0^r d\hat{r} \hat{r}^2 \left(\mathfrak{g}\rho(\hat{r}) + f^2 W W'(a')^2\right) \tag{154}$$

using the boundary condition $\phi'(0) \equiv 0$ coming from spherical symmetry. In a standard QBD theory, the last term is not present and the integral can be solved exactly for $\phi'(R)$ noticing that

$$M = 4\pi \int_0^R dr r^2 \rho(r) \,, \tag{155}$$

where M is the Sun mass. Since

$$\frac{1}{M_p^2} = 8\pi G \,, \tag{156}$$

one obtains

$$\phi'(R) = \frac{2\mathfrak{g} G M}{R^2} \,. \tag{157}$$

Comparing this result with (153) shows that the unscreened parameter is

$$L_0 = 2\mathfrak{g} G M \,. \tag{158}$$

Interestingly enough, looking at (152) and (158), notice how we got the same result as in (88) for a point source and massless scalar.

To solve the full equation of motion (149), we need first to formalize the behavior of a in the narrow width $R - l < r < R$. We approximate it with a step-function

$$a(r) = a_- + (a_+ - a_-)\Theta(r - R), \quad a'(r) = \Delta a \delta(r - R), \quad \Delta a \equiv (a_+ - a-) \tag{159}$$

with

$$\Theta(x) \equiv \lim_{l \to 0} \frac{1}{2} \left(1 + \tanh\left(\frac{x}{l}\right)\right), \quad \Theta'(x) = \delta(x), \quad \delta(0) = \frac{1}{2l} \,. \tag{160}$$

The last equality lets us write

$$\delta^2(r-R) = \delta(r-R)\delta(0) = \frac{1}{2l}\delta(r-R)\,, \tag{161}$$

which is necessary to convert (149) into

$$M_p^2\left(r^2\phi'\right)' = r^2\mathfrak{g}\rho + f^2WW'\frac{r^2}{2l}(\Delta a)^2\delta(r-R)\,. \tag{162}$$

Integrating both sides gives

$$\begin{aligned} M_p^2\int_{R-l}^{R} dr\left(r^2\phi'\right)' &= M_p^2\left(\left(r^2\phi'\right)_R - \left(r^2\phi'\right)_{R-l}\right) \\ &= M_p^2\left(R^2\,\phi'|_R - (R-l)^2\,\phi'|_{R-l}\right) \\ &\simeq M_p^2R^2\left(\phi'_{\text{ext}}|_R - \phi'|_{R-l}\right) \end{aligned} \tag{163}$$

and

$$\int_{R-l}^{R} dr r^2\mathfrak{g}\rho + \int_{R-l}^{R} dr f^2WW'\frac{r^2}{2l}(\Delta a)^2\delta(r-R) = f^2W_sW_s'\frac{R^2}{2l}(\Delta a)^2\,, \tag{164}$$

where the first integral in (164) vanishes for continuity of the integrand and the subscript s denotes evaluation at $r=R$. Combining the two sides back gives the jump condition

$$\phi'_{\text{ext}}(R) = \phi'(R-l) + \frac{f^2}{M_p^2}\frac{W_sW_s'}{2l}(\Delta a)^2\,, \tag{165}$$

which can be turned into the condition on L

$$L = L_0 + \frac{f^2}{M_p^2}W_sW_s'\frac{R^2}{2l}(\Delta a)^2 \tag{166}$$

by recalling that

$$\phi'_{\text{ext}}(R) = \frac{L}{R^2}, \phi'(R-l) \simeq \phi'(R) = \frac{2\mathfrak{g}GM}{R^2} = \frac{L_0}{R^2}\,. \tag{167}$$

To quantify the amount of screening provided by the saxion-axion coupling, it is convenient to look at the ratio L/L_0, which from (166) can easily be expressed as

$$\frac{L}{L_0} = 1 + \frac{\frac{f^2}{M_p^2}\frac{R^2}{2l}(\Delta a)^2}{L_0}W_sW_s'\,. \tag{168}$$

To achieve screening, we need this ratio to be smaller than 1.

Given the presence of $W_s(\phi)W_s'(\phi)$, (168) is not fully determined yet, but has a dependence on the integration parameter $\phi(R) \equiv \phi_s$. One chooses to fix its value by minimizing the energy of the whole system. Outside the Sun, the energy is given by

$$\begin{aligned} E_{\text{ext}} &= 4\pi M_p^2 \int_R^{+\infty} dr r^2 \frac{1}{2}(\phi_{\text{ext}}')^2 = 4\pi M_p^2 \int_R^{+\infty} dr r^2 \frac{1}{2}\frac{L^2}{r^4} = 2\pi M_p^2 \frac{L^2}{R} \\ &= \frac{L^2}{4GR} , \end{aligned} \tag{169}$$

while inside by

$$E_{\text{in}} = 4\pi \int_0^R dr r^2 \left(\frac{1}{2} f^2 W^2 (a')^2 + \frac{1}{2} M_p^2 (\phi')^2 \right) \simeq \pi f^2 \frac{R^2}{l} (\Delta a)^2 W_s^2 + E_0 , \tag{170}$$

using the narrow width approximation for the axion gradient. E_0 comes from the saxion gradient and is independent of ϕ_s. Overall,

$$\begin{aligned} \frac{4G}{R} E_{\text{tot}} &= \frac{4G}{R}(E_{\text{ext}} + E_{\text{in}}) \\ &= \frac{f^2}{M_p^2}\frac{R}{2l}(\Delta a)^2 W_s^2 + \left(\frac{L_0}{R} + \frac{f^2}{M_p^2}\frac{R}{2l}(\Delta a)^2 W_s W_s' \right)^2 + \frac{4G}{R} E_0 \\ &= y(\phi_s) + \left(B + \frac{1}{2} y'(\phi_s) \right)^2 + const. , \end{aligned} \tag{171}$$

where we defined

$$y(\phi_s) = \frac{f^2}{M_p^2}\frac{R}{2l}(\Delta a)^2 W_s^2, \quad B = \frac{L_0}{R} . \tag{172}$$

(172) lets us rewrite (168) as

$$\frac{L}{L_0} = 1 + \frac{y'(\phi_s)}{2B} . \tag{173}$$

Recalling that L_0 and $\mathfrak{g}$ are directly proportional through (158), one can introduce and effective coupling $\mathfrak{g}_{\text{eff}}$ such that $L \equiv 2\mathfrak{g}_{\text{eff}} GM$ and consequently

$$\frac{L}{L_0} = \frac{\mathfrak{g}_{\text{eff}}}{\mathfrak{g}} . \tag{174}$$

This allows to interpret the screening as the weakening of the saxion-SM coupling. The absence of observable fifth-forces imposes $\mathfrak{g}_{\text{eff}} \lesssim 10^{-3}$ [33] (see Fig. 7).

This is as far as our general framework can take us. To continue our analysis, one needs to assume functional forms for $W^2(\phi)$.

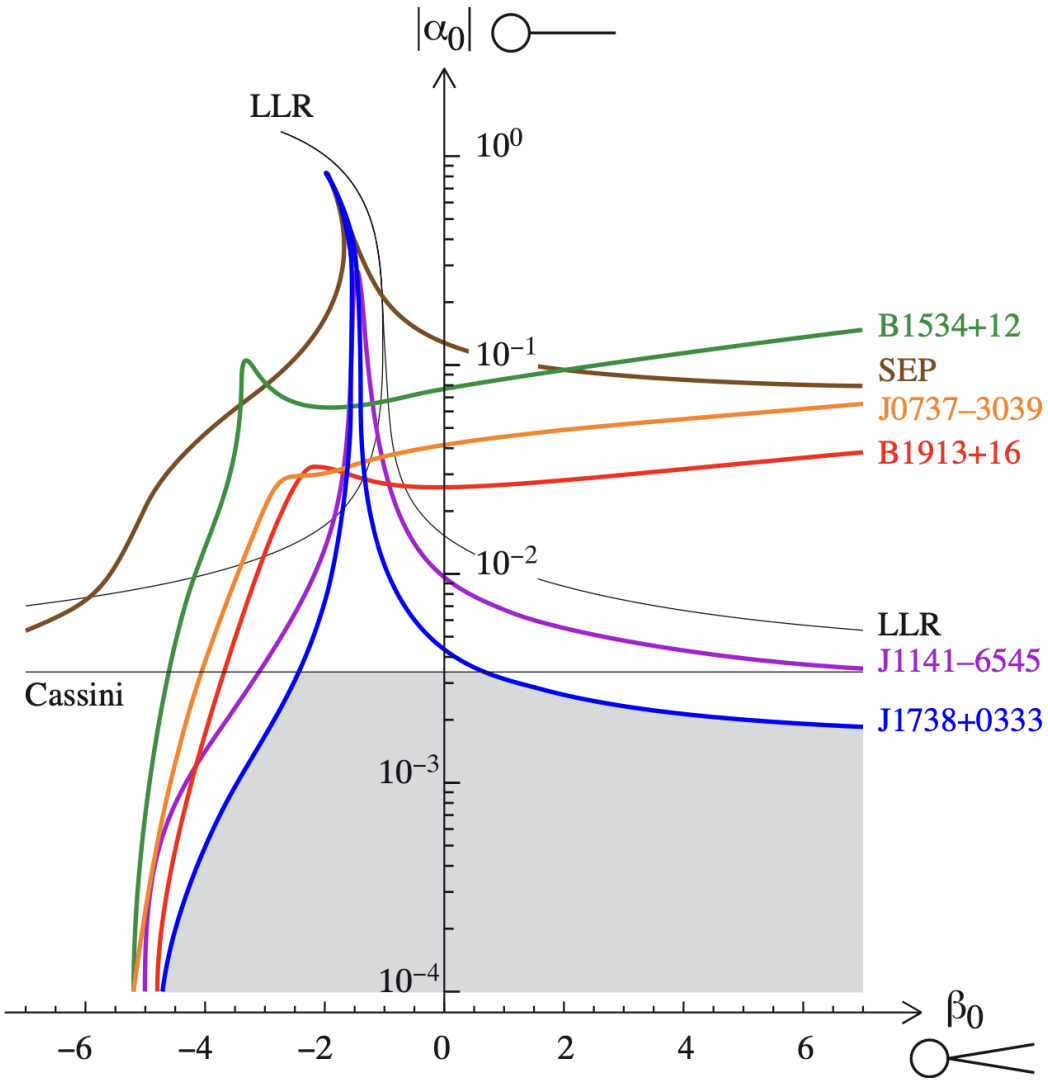

Figure 7: Solar-system and binary pulsar 1-σ constraints on the matter-scalar coupling constants α_0 and β_0 assuming $\ln A(\phi) = \ln A(\phi_0) + \alpha_0(\phi - \phi_0) + \frac{1}{2}\beta_0(\phi - \phi_0)^2 + ...$ Note that a logarithmic scale is used for the vertical axis $|\alpha_0|$, i.e. that GR ($\alpha_0 = \beta_0 = 0$) is sent at infinite distance down this axis. LLR stands for lunar laser ranging, Cassini for the measurement of a Shapiro time-delay variation in the Solar System and SEP for tests of the Strong Equivalence Principle using a set of neutron star-white dwarf low-eccentricity binaries. The allowed region is shaded and it includes GR. Figure from [33].

3.5 Exponential W^2

Here we consider the case

$$W(\phi) \equiv W_0 e^{-\frac{1}{2}\xi\phi} \to y(\phi_s) \propto e^{-\xi\phi_s}, \quad y' = -\xi y \,. \tag{175}$$

It follows that the total energy is

$$\frac{4G}{R} E_{\text{tot}} = y(\phi_s) + \left(B - \frac{1}{2}\xi y(\phi_s) \right)^2 + const. \tag{176}$$

Since $y(\phi_s)$ is monotone, one can equivalently minimize E_{tot} with respect to it in place of ϕ_s. Direct calculations show the energy minimum to be at

$$y = \frac{2B}{\xi}\left(1 - \frac{1}{\xi B}\right) \,. \tag{177}$$

Plugging (177) into (173) gives

$$\frac{L}{L_0} = 1 - \frac{\xi y}{2B} = \frac{1}{\xi B} = \frac{R}{2\xi \mathfrak{g} GM} \,. \tag{178}$$

For the Sun, $R/GM \sim 10^{-6}$ [1]. Starting from a coupling $\mathfrak{g} \sim \mathcal{O}(1)$, this means that one needs $\xi \gtrsim 10^9$ to reach the required amount of screening.

3.6 Quadratic W^2

Another interesting possibility is the case

$$W^2(\phi) \equiv W_0^2 + \frac{W_1^2}{2}(\phi - \phi_0)^2 \,, \tag{179}$$

from which it follows that

$$y(\phi_s) = y_0 + \frac{y_1}{2}(\phi - \phi_0)^2 \tag{180}$$

with

$$y_i \equiv \frac{f^2}{M_p^2}\frac{R}{2l}(\Delta a)^2 W_i^2 \,. \tag{181}$$

Deriving (180) gives

$$y'(\phi_s) = y_1(\phi - \phi_0) \,. \tag{182}$$

From (171) one obtains

$$\frac{4G}{R} E_{\text{tot}} = y_0 + \frac{y_1}{2}(\phi - \phi_0)^2 + \left(B + \frac{y_1}{2}(\phi - \phi_0) \right)^2 \,, \tag{183}$$

which can be extremized with respect to $(\phi_s - \phi_0)$ to find the minimum

$$\phi - \phi_0 = -\frac{B}{1 + \frac{y_1}{2}} \,. \tag{184}$$

Combining (173), (182) and (184), we obtain

$$\frac{L}{L_0} = 1 - \frac{y_1 \frac{B}{1+\frac{y_1}{2}}}{2B} = \frac{1}{1 + \frac{y_1}{2}} = \frac{1}{1 + \frac{1}{4}\frac{f^2}{M_p^2}\frac{R}{l}(\Delta a)^2 W_1^2} \,. \tag{185}$$

Therefore, to have significant amount of screening, $l/R \ll (\Delta a)^2 W_1^2 f^2/M_p^2$ is required, which is likely to be valid in the narrow-width limit, since one expects $W_1^2 f^2/M_p^2$ to be of order unity.

4 The Axio-Chameleon Mechanism in String Theory

Here we study potential embeddings of the axio-chameleon screening mechanism in String Theory. In particular, closed string moduli give rise to the exponential form of W^2, while brane-position moduli can be used to implement the quadratic form of W^2. First, we discuss how closed string moduli are actually not good candidates for this type of screening. We then move on to the much more promising second option.

4.1 Closed String Moduli

In the context of Supergravity, complexified closed string moduli are associated to Kähler potentials of the form

$$K = -n\ln(\Phi + \bar{\Phi}) \tag{186}$$

with $n = 1, 2, 3$ when dealing with the axiodilaton, some inner Kähler modulus or the volume modulus respectively. We obtain the metric of the target space using

$$\mathcal{G}_{\Phi\bar{\Phi}} = K_{\Phi\bar{\Phi}} = \frac{n}{(\Phi + \bar{\Phi})^2} \, . \tag{187}$$

The saxion-axion pair can be seen by turning the complex field into two real fields using cartesian decomposition

$$\Phi \equiv \phi + i\theta \, . \tag{188}$$

This guarantees, as opposed to polar decomposition, that K has no dependence on θ, as one needs from an axion.

The generalized kinetic term [34] is

$$\begin{aligned} K_{\Phi\bar{\Phi}}\partial_\mu\Phi\partial^\mu\bar{\Phi} &= \frac{n}{(\Phi + \bar{\Phi})^2}\partial_\mu\Phi\partial^\mu\bar{\Phi} = \frac{n}{(2\phi)^2}(\partial_\mu\phi + i\partial_\mu\theta)(\partial^\mu\phi - i\partial^\mu\theta) \\ &= \frac{n}{4\phi^2}(\partial_\mu\phi\partial^\mu\phi + \partial_\mu\theta\partial^\mu\theta) \, . \end{aligned} \tag{189}$$

Using the redefinition

$$\sqrt{\frac{n}{2}}\frac{\partial_\mu\phi}{\phi} \equiv \partial_\mu\chi \to \chi = \sqrt{\frac{n}{2}}\ln(\phi), \quad \phi = e^{\sqrt{\frac{2}{n}}\chi} \tag{190}$$

to put the saxion in canonical form, we find (see [35] for the axiodilaton case)

$$L \supset -\sqrt{-g}M_p^2 K_{\Phi\bar{\Phi}}\partial_\mu\Phi\partial^\mu\bar{\Phi} = -\sqrt{-g}\left(\frac{M_p^2}{2}\partial_\mu\chi\partial^\mu\chi + \frac{M_p^2}{2}\frac{n}{2}e^{-2\sqrt{\frac{2}{n}}\chi}\partial_\mu\theta\partial^\mu\theta\right) \, . \tag{191}$$

By comparing it with (175), we notice that $2\sqrt{2/n}$ plays the role of ξ. Recalling that ξ has to be at least of order 10^9 if $\mathfrak{g} = O(1)$ in order to get a significant amount of screening, we easily realize that this cannot be achieved in the framework of String Theory.

We do need to point out that these results were obtained assuming a specific Weyl rescaling between the Einstein and Jordan metric

$$\tilde{g}_{\mu\nu} = e^{2\mathfrak{g}\chi} g_{\mu\nu} \,, \tag{192}$$

which results in a constant coupling between the saxion and SM matter. One could in principle consider different types of coupling (as we end up doing for the open string case), hoping to get a more string-friendly constraint on ξ. However a shift of 9 orders of magnitude seems unlikely.

4.2 Brane-Position Moduli

We recall our final result from the section on D-branes: the action

$$\begin{aligned} S = \frac{M_p^2}{2}\int d^4x\sqrt{-g_4}R_4 - \frac{2\pi}{g_s l_s^4}\int d^4x\sqrt{-g_4}\frac{1}{2}\frac{\mathcal{V}_W^0}{\mathcal{V}_W}\mathcal{V}^{\frac{1}{3}} g_{mn}\partial_\mu y^m \partial^\mu y^n \\ + S_{\mathsf{SM}}(\tilde{g}_{\mu\nu}) \,. \end{aligned} \tag{193}$$

By taking the singular conifold as the compactified metric

$$\begin{aligned} ds^2 =& d\rho^2 + \rho^2\left[\frac{1}{9}(d\psi + \mathsf{cos}\theta_1 d\phi_1 + \mathsf{cos}\theta_2 d\phi_2)^2 + \frac{1}{6}(d\theta_1^2 + \mathsf{sin}^2\theta_1 d\phi_1^2)\right. \\ &\left. + \frac{1}{6}(d\theta_2^2 + \mathsf{sin}^2\theta_2 d\phi_1^2)\right] \,, \end{aligned} \tag{194}$$

we obtain

$$\begin{aligned} & -\frac{2\pi}{g_s l_s^4}\int d^4x\sqrt{-g_4}\frac{1}{2}\frac{\mathcal{V}_W^0}{\mathcal{V}_W}\mathcal{V}^{\frac{1}{3}} g_{mn}\partial_\mu y^m \partial^\mu y^n \\ &= -\frac{2\pi}{g_s l_s^4}\int d^4x\sqrt{-g_4}\frac{1}{2}\frac{\mathcal{V}_W^0}{\mathcal{V}_W}\mathcal{V}^{\frac{1}{3}}\left(\partial_\mu\rho\partial^\mu\rho + n\rho^2\partial_\mu a\partial^\mu a\right) \end{aligned} \tag{195}$$

with n a numerical coefficient dependent on how we define the axion a starting from the five angles ψ, ϕ_1, ϕ_2, θ_1, θ_2. As an example, if we assume ψ to be our axion, then $n = 1/9$. It is worth noticing that in general $n \neq 1$; for a detailed discussion on the matter, see Appendix B. Clearly, after each definition of a, one must verify that field is indeed a pseudo-scalar and enjoys shift symmetry.

Redefining the radial-position modulus into its canonical form through

$$\phi = \sqrt{\frac{1}{M_p^2}\frac{2\pi}{g_s l_s^4}\frac{\mathcal{V}_W^0}{\mathcal{V}_W}\mathcal{V}^{\frac{1}{3}}}\rho = \sqrt{\frac{l_s^2}{4\pi\mathcal{V}_W^0}\frac{2\pi}{g_s l_s^4}\frac{\mathcal{V}_W^0}{\mathcal{V}_W}\mathcal{V}^{\frac{1}{3}}}\rho = \sqrt{\frac{\mathcal{V}^{\frac{1}{3}}}{2g_s\mathcal{V}_W}}\frac{\rho}{l_s} \,, \tag{196}$$

we obtain

$$\begin{aligned} &-\frac{2\pi}{g_s l_s^4}\int d^4x\sqrt{-g_4}\frac{1}{2}\frac{\mathcal{V}_W^0}{\mathcal{V}_W}\mathcal{V}^{\frac{1}{3}}\partial_\mu\rho\partial^\mu\rho \\ &=-\frac{M_p^2}{2}\int d^4x\sqrt{-g_4}\partial_\mu\phi\partial^\mu\phi\,, \end{aligned} \tag{197}$$

$$\begin{aligned} &-\frac{2\pi}{g_s l_s^4}\int d^4x\sqrt{-g_4}\frac{1}{2}\frac{\mathcal{V}_W^0}{\mathcal{V}_W}\mathcal{V}^{\frac{1}{3}}n\rho^2\partial_\mu a\partial^\mu a \\ &=-\int d^4x\sqrt{-g_4}\frac{2\pi}{g_s l_s^4}\frac{1}{2}\frac{\mathcal{V}_W^0}{\mathcal{V}_W}\mathcal{V}^{\frac{1}{3}}n\left(\frac{2g_s\mathcal{V}_W}{\mathcal{V}^{\frac{1}{3}}}l_s^2\right)\phi^2\partial_\mu a\partial^\mu a \\ &=-\int d^4x\sqrt{-g_4}\frac{1}{2}\frac{4\pi}{l_s^2}\mathcal{V}_W^0 n\phi^2\partial_\mu a\partial^\mu a \\ &=-\int d^4x\sqrt{-g_4}\frac{1}{2}f^2\phi^2\partial_\mu a\partial^\mu a \end{aligned} \tag{198}$$

with f defined as

$$f=\sqrt{\frac{4\pi}{l_s^2}\mathcal{V}_W^0 n}=M_p\sqrt{n} \tag{199}$$

and finally the action

$$\begin{aligned} S=&\int d^4x\sqrt{-g_4}\left(\frac{M_p^2}{2}R_4-\frac{M_p^2}{2}\partial_\mu\phi\partial^\mu\phi-\frac{1}{2}f^2\phi^2\partial_\mu a\partial^\mu a-V(a)\right) \\ &+S_{\text{SM}}(\tilde{g}_{\mu\nu})\,. \end{aligned} \tag{200}$$

Notice that f has mass dimension 1 as expected.

In (200) we assumed the saxion potential to be negligible, i.e. flat, while $V(a)$ enjoys shift symmetry. It would be desirable to back up these claims by studying the fluxes living on the conifold. In this thesis, we provide only qualitative arguments, leaving more rigorous demonstrations to future research. Let us start by addressing the flatness of the saxion potential. This is what makes ϕ light and in need of screening in the first place. Therefore, there is no point in studying the axio-chameleon screening mechanism for a massive saxion, since the fifth-forces would already be short-range. Moreover, it has already been shown that ϕ can be used as the inflaton [4][36][37][38][10] or quintessence field [10][39], for which the flatness of the potential is mandatory. One could then, for example, interpret ϕ as the quintessence field, currently living in the flat region of the potential, and aim to use the screening mechanism to explain the absence of observable fifth-forces. Regarding the axion, the Kähler potential that sources the singular conifold metric has no dependence on the angular coordinates [11]. This is no longer true after introducing warping, unless the stack of branes sourcing it is placed at the tip, preserving the symmetry of the geometry. However, the general case

still preserve a discrete shift-symmetry of the angles, due to their intrinsic periodicity. For this reason, we believe the conifold angles, or combinations of them, to be good axion candidates.

4.2.1 Generalization to a Field-Dependent Coupling Constant

By comparing (200) and (144), we notice that we have reached the same setup for the screening mechanism as the one presented in [1], with quadratic W^2. The only difference lays in the Weyl factor and, therefore, in the saxion-SM coupling. Indeed, while in [1] the authors assume

$$\tilde{g}_{\mu\nu} = A^2(\phi) g_{\mu\nu} = e^{2\mathfrak{g}\phi} g_{\mu\nu} \,, \tag{201}$$

we keep a more general scope and for the moment consider a generic non-constant $\mathfrak{g}(\phi)$. We present now the implications of this generalization. In doing so, we also re-define all relevant elements to be dimensionless in preparation for the soon to come numerical analysis.

Let us start again from the saxion equation of motion one obtains from the action

$$r^2\phi'' + 2r\phi' - \frac{r^2}{M_p^2}\rho\mathfrak{g}(\phi) - \bar{f}^2 r^2 \phi (a')^2 = 0 \,, \tag{202}$$

where $\mathfrak{g} = \mathfrak{g}(\phi)$, $\rho = const.$ for simplicity, $\bar{f} \equiv f/M_p = \sqrt{n}$ and ϕ and a are already dimensionless. We substitute also r with its dimensionless counterpart through the definitions

$$r, \rho \longrightarrow \bar{r} = M_p r, \; \bar{\rho} = \frac{\rho}{M_p^4} \longrightarrow \tilde{r} = \bar{r}\sqrt{\bar{\rho}} = \frac{r\sqrt{\rho}}{M_p} = r\sqrt{\rho}\sqrt{\frac{l_p}{M_p}} \tag{203}$$

and (202) becomes

$$\tilde{r}^2\phi'' + 2\tilde{r}\phi' - \tilde{r}^2\mathfrak{g}(\phi) - \bar{f}^2\tilde{r}^2\phi(a')^2 = 0 \,. \tag{204}$$

Again, we solve (204) both inside and outside the Sun, as well as in the narrow width at the boundary. Outside the Sun, the terms representing interaction with the SM and the axion gradient vanish, simplifying the equation of motion to

$$\tilde{r}^2\phi'' + 2\tilde{r}\phi' = 0 \tag{205}$$

or equivalently

$$(\tilde{r}^2\phi')' = 0 \,. \tag{206}$$

Introducing $\tilde{L}$ as

$$(\tilde{r}^2\phi')_{\tilde{r}=\tilde{R}} = \tilde{L} \,, \tag{207}$$

we find the solution

$$\phi_{\text{ext}}(\tilde{r}) = \phi_\infty - \frac{\tilde{L}}{\tilde{r}}\,, \tag{208}$$

where ϕ_∞ is the value of the field at infinite distance from the Sun.

Inside the Sun we only have

$$\tilde{r}^2\phi'' + 2\tilde{r}\phi' - \tilde{r}^2\mathfrak{g}(\phi) = 0\,, \tag{209}$$

since we assume the axion gradient to be non-null only in a thin region at the boundary. Through integration, (209) is equivalent to

$$\phi'(\tilde{r}) = \frac{1}{\tilde{r}^2}\int_0^{\tilde{r}} dr r^2\mathfrak{g}(\phi)\,, \tag{210}$$

from which one finds

$$\tilde{L}_0 = (\tilde{r}^2\varphi')_{\tilde{r}=\tilde{R}} = \int_0^{\tilde{R}} d\tilde{r}\tilde{r}^2\mathfrak{g}(\phi)\,, \tag{211}$$

where $\tilde{R} \simeq 7*10^{-4}$ is the dimensionless Sun radius. Unlike in [1], (210) and (211) cannot be solved analytically in general, neither will they be for the specific case we are about to consider.

In the narrow width, all terms of (204) are relevant. In narrow-width approximation, we use

$$a'(\tilde{r}) = \Delta a\delta(\tilde{r} - \tilde{R}) \tag{212}$$

to turn (204) into

$$\tilde{r}^2\phi'' + 2\tilde{r}\phi' = \tilde{r}^2\mathfrak{g}(\phi) + \bar{f}^2\frac{\tilde{r}^2}{2\tilde{l}}\phi(\Delta a)^2\delta(\tilde{r} - \tilde{R})\,, \tag{213}$$

where we used

$$\delta^2(\tilde{r} - \tilde{R}) = \delta(\tilde{r} - \tilde{R})\delta(0) \tag{214}$$

and introduced the width thickness through

$$\delta(0) = \frac{1}{2\tilde{l}}\,. \tag{215}$$

Let us integrate both sides separately. We have

$$\begin{aligned}\int_{\tilde{R}-\tilde{l}}^{\tilde{R}} d\tilde{r}\left(\tilde{r}^2\phi'' + 2\tilde{r}\phi'\right) &= \int_{\tilde{R}-\tilde{l}}^{\tilde{R}} d\tilde{r}\left(\tilde{r}^2\phi'\right)' = \left(\tilde{r}^2\phi'\right)_{\tilde{R}} - \left(\tilde{r}^2\phi'\right)_{\tilde{R}-\tilde{l}} \\ &= \tilde{R}^2\ \phi'|_{\tilde{R}} - (\tilde{R} - \tilde{l})^2\ \phi'|_{\tilde{R}-\tilde{l}} \simeq \tilde{R}^2\left(\phi'_{\text{ext}}|_{\tilde{R}} - \phi'|_{\tilde{R}-\tilde{l}}\right)\end{aligned} \tag{216}$$

and

$$\int_{\tilde{R}-\tilde{l}}^{\tilde{R}} d\tilde{r}\tilde{r}^2\mathfrak{g}(\phi) + \int_{\tilde{R}-\tilde{l}}^{\tilde{R}} d\tilde{r}\bar{f}^2\frac{\tilde{r}^2}{2\tilde{l}}\phi(\Delta a)^2\delta(\tilde{r} - \tilde{R}) = \bar{f}^2\frac{\tilde{R}^2}{2\tilde{l}}\phi_s(\Delta a)^2\,, \tag{217}$$

where the first integral is subleading for small $\tilde{l}$ for continuity of $\phi(\tilde{r})$. Finally, we obtain the jump condition on the derivative of ϕ

$$\phi'_{\text{ext}}(\tilde{R}) = \phi'(\tilde{R}-\tilde{l}) + \bar{f}^2\frac{\phi_s}{2\tilde{l}}(\Delta a)^2\,, \tag{218}$$

which equivalently gives the relation

$$\tilde{L} = \tilde{L}_0 + \bar{f}^2\frac{\tilde{R}^2}{2\tilde{l}}(\Delta a)^2\phi_s\,. \tag{219}$$

Similarly to what we did in Chapter 3, we quantify the screening through the ratio

$$\frac{L}{L_0} = \frac{\tilde{L}}{\tilde{L}_0} = 1 + \frac{\bar{f}^2\frac{\tilde{R}^2}{\tilde{l}}(\Delta a)^2}{2\tilde{L}_0}\phi_s\,. \tag{220}$$

The first equation becomes apparent once one realizes that

$$\begin{aligned} L_0 &= \frac{1}{M_p^2}\int_0^R drr^2\rho\mathfrak{g}(\phi) = \frac{1}{M_p^2}\int_0^{\frac{M_p}{\sqrt{\rho}}\tilde{R}} d\left(\frac{M_p}{\sqrt{\rho}}\tilde{r}\right)\left(\frac{M_p}{\sqrt{\rho}}\tilde{r}\right)^2\rho\mathfrak{g}(\phi) \\ &= \frac{1}{M_p^2}\left(\frac{M_p}{\sqrt{\rho}}\right)^3\int_0^{\tilde{R}} d\tilde{r}\tilde{r}^2\rho\mathfrak{g}(\phi) = \frac{M_p}{\sqrt{\rho}}\tilde{L}_0 \end{aligned} \tag{221}$$

and

$$\begin{aligned} L &= L_0 + \bar{f}^2\frac{R^2}{2l}(\Delta a)^2\phi_s = \frac{M_p}{\sqrt{\rho}}\tilde{L}_0 + \bar{f}^2\frac{\left(\frac{M_p}{\sqrt{\rho}}\tilde{R}\right)^2}{2\left(\frac{M_p}{\sqrt{\rho}}\tilde{l}\right)}(\Delta a)^2\phi_s \\ &= \frac{M_p}{\sqrt{\rho}}\left(\tilde{L}_0 + \bar{f}^2\frac{\tilde{R}^2}{2\tilde{l}}(\Delta a)^2\phi_s\right) = \frac{M_p}{\sqrt{\rho}}\tilde{L}\,. \end{aligned} \tag{222}$$

An important observation can be made here, which is going to guide us in the realization of our brane setup on the conifold. In order to have screening, i.e. $L/L_0 < 1$, the second term in (220) needs to be negative. In [1], this was possible because at the energy minimum the field would assume a negative value. This cannot be true for our stringy model, since ϕ represents the radial coordinate on the conifold, which is always non-negative. Our only hope is for L_0, and therefore $\mathfrak{g}(\phi)$, to be negative. Therefore, we must build a setup where that is the case. We will put this insight to good use in the next section; for now, we continue our generalization of the screening mechanism, focusing on the energy profile and minimization.

Similarly to Chapter 3, the total energy is given by the sum of the energy inside and outside the Sun, with

$$\begin{aligned} E_{\text{ext}} &= 4\pi M_p^2 \int_R^{+\infty} dr r^2 \frac{1}{2}(\phi'_{\text{ext}})^2 = \frac{4\pi M_p^3}{\sqrt{\rho}} \int_{\tilde{R}}^{+\infty} d\tilde{r}\tilde{r}^2 \frac{1}{2}(\phi'_{\text{ext}})^2 \\ &= \frac{4\pi M_p^3}{\sqrt{\rho}} \int_{\tilde{R}}^{+\infty} d\tilde{r}\tilde{r}^2 \frac{1}{2}\frac{\tilde{L}^2}{\tilde{r}^4} = \frac{2\pi M_p^3}{\sqrt{\rho}} \frac{\tilde{L}^2}{\tilde{R}} \end{aligned} \tag{223}$$

and

$$\begin{aligned} E_{\text{in}} &= \pi f^2 \frac{R^2}{l}(\Delta a)^2 \phi_s^2 + 4\pi M_p^2 \int_0^R dr r^2 \frac{1}{2}(\phi')^2 \\ &= \frac{2\pi M_p^3}{\sqrt{\rho}} \left(\bar{f}^2 \frac{\tilde{R}^2}{2\tilde{l}}(\Delta a)^2 \phi_s^2 + \int_0^{\tilde{R}} d\tilde{r}\tilde{r}^2 (\phi')^2 \right) , \end{aligned} \tag{224}$$

where to go from dimensionful to dimensionless lengths we used similar steps to those in (221) and (222). In the case of constant $\mathfrak{g}$, the last term of (224) would not be relevant for the energy minimization, since it would not depend on ϕ_s. However, this is not true in general. After summing we find

$$\begin{aligned} \frac{\sqrt{\rho}}{2\pi M_p^3 \tilde{R}} E_{\text{tot}} &= \frac{\sqrt{\rho}}{2\pi M_p^3 \tilde{R}} (E_{\text{ext}} + E_{\text{in}}) \\ &= \bar{f}^2 \frac{\tilde{R}}{2\tilde{l}}(\Delta a)^2 \phi_s^2 + \left(\frac{1}{\tilde{R}} \int_0^{\tilde{R}} d\tilde{r}\tilde{r}^2 \mathfrak{g}(\phi) + \bar{f}^2 \frac{\tilde{R}}{2\tilde{l}}(\Delta a)^2 \phi_s \right)^2 \\ &+ \frac{1}{\tilde{R}} \int_0^{\tilde{R}} d\tilde{r}\tilde{r}^2 (\phi')^2 \\ &= \frac{y_1}{2}\phi_s^2 + \left(B(\phi_s) + \frac{y_1}{2}\phi_s \right)^2 + I(\phi_s) \end{aligned} \tag{225}$$

with

$$y_1 = \bar{f}^2 \frac{\tilde{R}}{\tilde{l}}(\Delta a)^2, B(\varphi_s) = \frac{1}{\tilde{R}} \int_0^{\tilde{R}} d\tilde{r}\tilde{r}^2 \mathfrak{g}(\phi) = \tilde{R}\varphi'(\tilde{R}) = \frac{\tilde{L}_0}{\tilde{R}}, I(\varphi_s) = \frac{1}{\tilde{R}} \int_0^{\tilde{R}} d\tilde{r}\tilde{r}^2 (\varphi')^2. \tag{226}$$

Notice how y_1 is the same whether we use dimensionless or dimensionful lengths.

Using (226), (220) becomes

$$\frac{L}{L_0} = 1 + \frac{y_1}{2B(\phi_s)}\phi_s \, , \tag{227}$$

where ϕ_s is evaluated at the energy minimum.

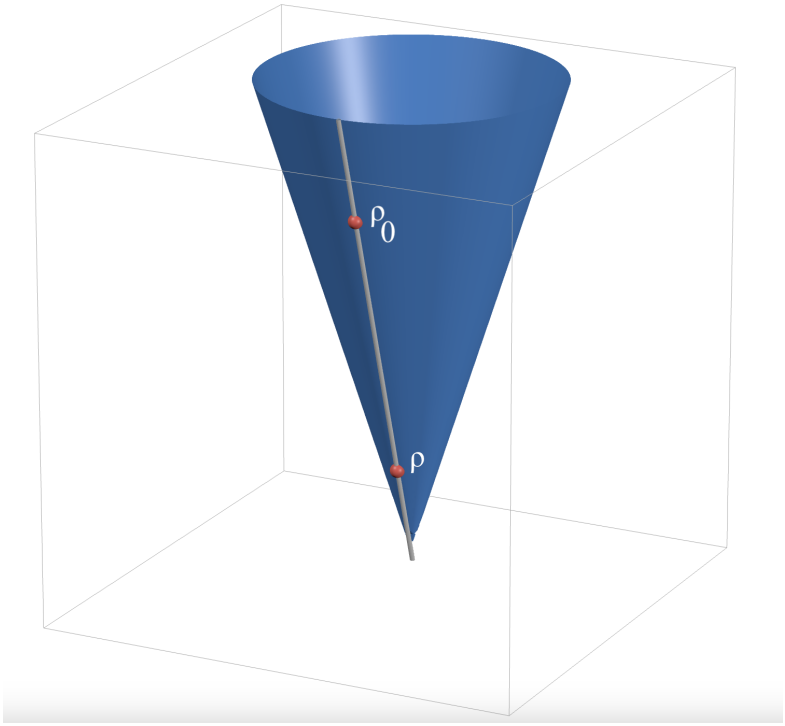

Figure 8: Pictorial representation of the brane setup on the conifold. The stack is stabilized at ρ_0, while the SM-brane can move in all directions and has radial coordinate ρ.

4.2.2 Brane setup on the conifold

We have already highlighted how, for the screening mechanism to work, we need $\mathfrak{g}(\phi)$ to be negative. Here we investigate what this implies for the brane setup on the conifold.

Recall that $\mathfrak{g}(\phi)$ comes from the Weyl factor through the relation

$$\mathfrak{g}(\phi) = \partial_\phi \ln A \,, \tag{228}$$

where A comes from

$$\tilde{g}_{\mu\nu} = A^2(\phi) g_{\mu\nu} \,. \tag{229}$$

For the open string model we found

$$\tilde{g}_{\mu\nu} = h^{-\frac{1}{2}} e^{2\omega} g_{\mu\nu} \to A = h^{-\frac{1}{4}} e^{\omega} \,. \tag{230}$$

Using properties of the logarithm, we can trace the following logical map

$$\mathfrak{g}(\phi) < 0 \iff \partial_\phi \ln A < 0 \iff \partial_\phi A < 0 \iff \partial_\phi h > 0 \,; \tag{231}$$

that is, the warping must increase with the radial coordinate at least in some region of the conifold. In the common scenario where the warping is sourced by a stack of branes and fractional branes at the tip of the conifold, the opposite is true. Therefore, we are led to consider a different setup. We imagine to stabilize a stack of branes at some radial position ρ_0, while the SM lives on a probe D3-/$\overline{\text{D3}}$-brane moving between 0 and ρ_0 and along the angular directions. For simplicity, we assume the stack and the probe brane to be almost aligned in the angular coordinates and to be practically separated only along the radial direction (see 8 and [40] for a more general solution). Starting from (59), this allows us to write the warp factor in the strong warping regime as

$$h = \frac{c^4}{(\rho - \rho_0)^4} = \frac{\bar{c}^4}{(\phi - \phi_0)^4} \,, \tag{232}$$

where we used (196) to go from ρ, ρ_0 to ϕ, ϕ_0 and all the multiplicative constants have been reabsorbed into $\bar{c}^4$.

Consequently,

$$A = \left(h^{-\frac{1}{2}} e^{2\omega}\right)^{\frac{1}{2}} = h^{-\frac{1}{4}} e^{\omega} = \frac{\phi - \phi_0}{\tilde{c}} \tag{233}$$

and

$$\mathfrak{g}(\phi) = \frac{1}{\phi - \phi_0}, \quad 0 < \phi < \phi_0 \,, \tag{234}$$

which is indeed negative. Since ϕ_0 is constant, it is convenient from now on to use the shifted field $\varphi = \phi - \phi_0$ in place of ϕ.

4.2.3 Numerical Analysis

Combining results from the last two sections, we obtain

$$\tilde{r}^2 \varphi'' + 2\tilde{r}\varphi' - \tilde{r}^2 \frac{1}{\varphi} - \bar{f}^2 \tilde{r}^2 (\varphi + \phi_0)(a')^2 = 0 \,, \tag{235}$$

$$\frac{L}{L_0} = \frac{\tilde{L}}{\tilde{L}_0} = 1 + \frac{y_1}{2B(\varphi_s)}(\varphi_s + \phi_0) \tag{236}$$

with

$$B(\varphi_s) = \frac{1}{\tilde{R}} \int_0^{\tilde{R}} d\tilde{r} \tilde{r}^2 \frac{1}{\varphi} = \tilde{R}\varphi'(\tilde{R}) = \frac{\tilde{L}_0}{\tilde{R}} \tag{237}$$

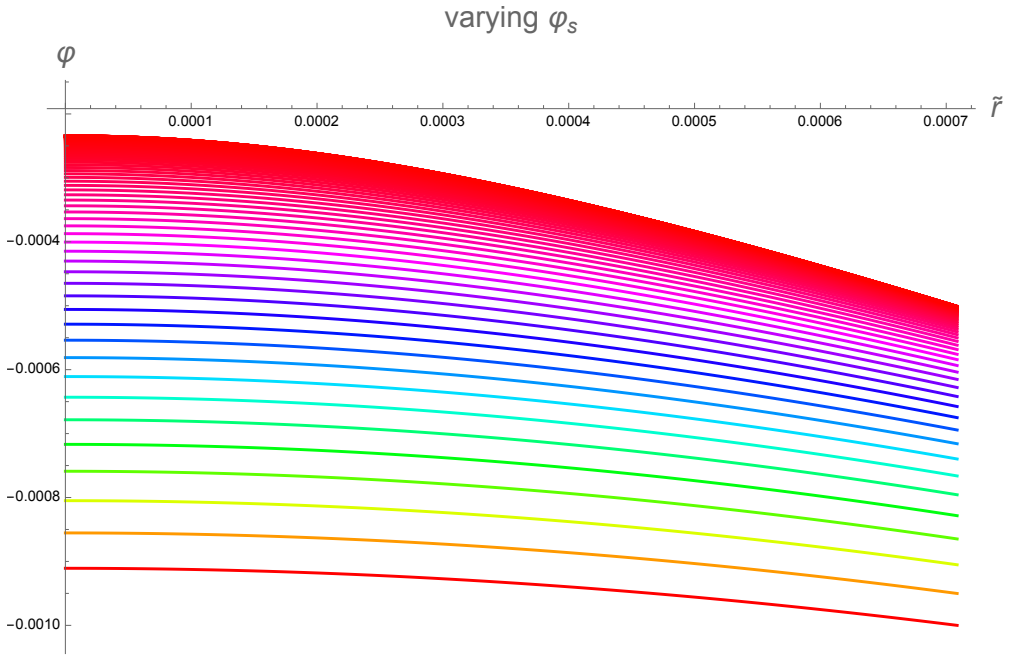

Figure 9: Numerical solutions of (239) for $\tilde{r} \in [0, \tilde{R}]$ and various φ_s.

and

$$\begin{aligned}\frac{\sqrt{\rho}}{2\pi M_p^3 \tilde{R}} E_{\text{tot}} &= \frac{\sqrt{\rho}}{2\pi M_p^3 \tilde{R}} (E_{\text{ext}} + E_{\text{in}}) \\ &= \bar{f}^2 \frac{\tilde{R}}{2\tilde{l}} (\Delta a)^2 (\varphi_s + \phi_0)^2 + \left(\frac{1}{\tilde{R}} \int_0^{\tilde{R}} d\tilde{r} \tilde{r}^2 \frac{1}{\varphi} + \bar{f}^2 \frac{\tilde{R}}{2\tilde{l}} (\Delta a)^2 (\varphi_s + \phi_0) \right)^2 \\ &+ \frac{1}{\tilde{R}} \int_0^{\tilde{R}} d\tilde{r} \tilde{r}^2 (\varphi')^2 \\ &= \frac{y_1}{2} (\varphi_s + \phi_0)^2 + \left(B(\varphi_s) + \frac{y_1}{2} (\varphi_s + \phi_0) \right)^2 + I(\varphi_s) \, .\end{aligned} \tag{238}$$

Our goal here is to find the energy profile and minimize it with respect to φ_s, in order to get an equation for the screening as a function of y_1 and ϕ_0. To do so, we need to express E_{tot} as an explicit function of φ_s. That is, we need at least an approximate dependence of φ on φ_s, which we can find by solving (235) numerically inside the Sun, i.e. neglecting the last term.

Plotting the numerical results of

$$\tilde{r}^2 \varphi'' + 2\tilde{r}\varphi' - \tilde{r}^2 \frac{1}{\varphi} = 0 \tag{239}$$

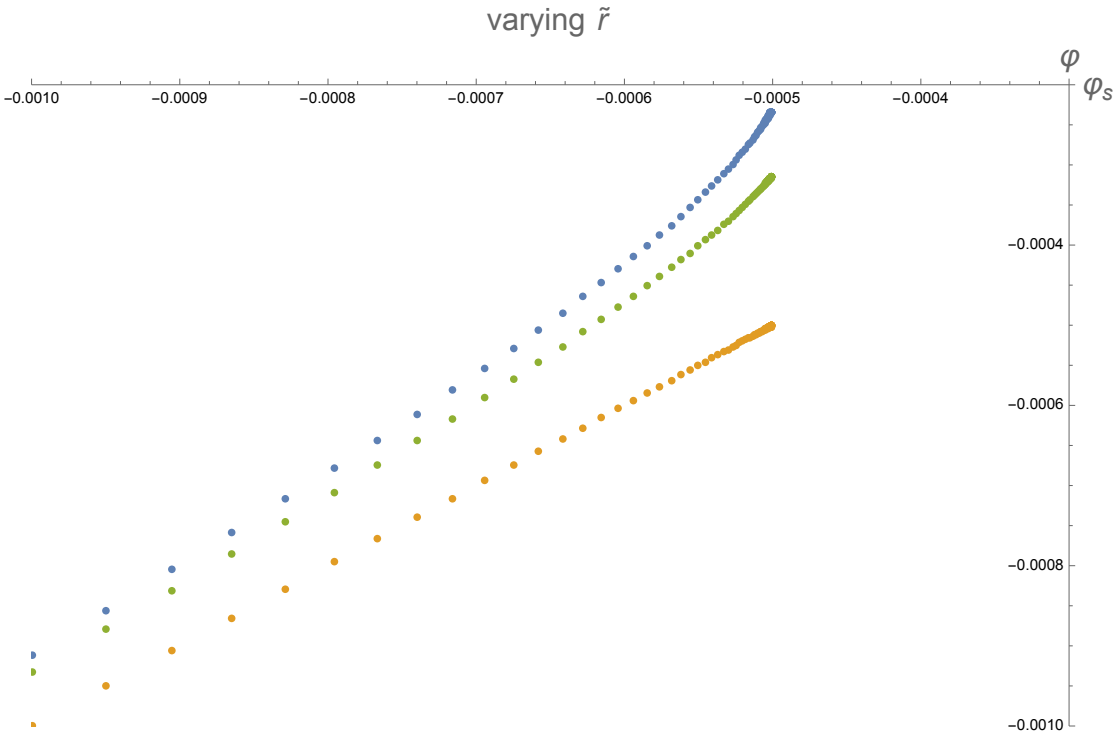

Figure 10: Numerical evaluation of $\varphi(\tilde{r}, \varphi_s)$ along φ_s for $\tilde{r} = 0$ (blue), $\tilde{r} = \tilde{R}/2$ (green) and $\tilde{r} = \tilde{R}$ (orange).

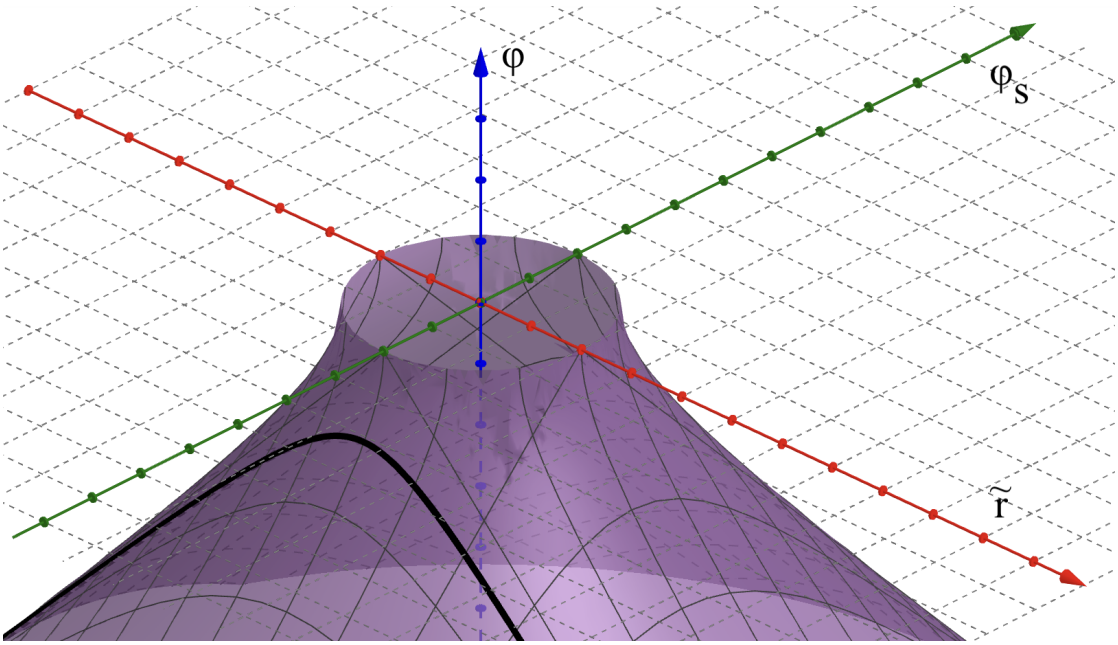

Figure 11: Hyperboloid given by (241) and φ at a fixed φ_s (black).

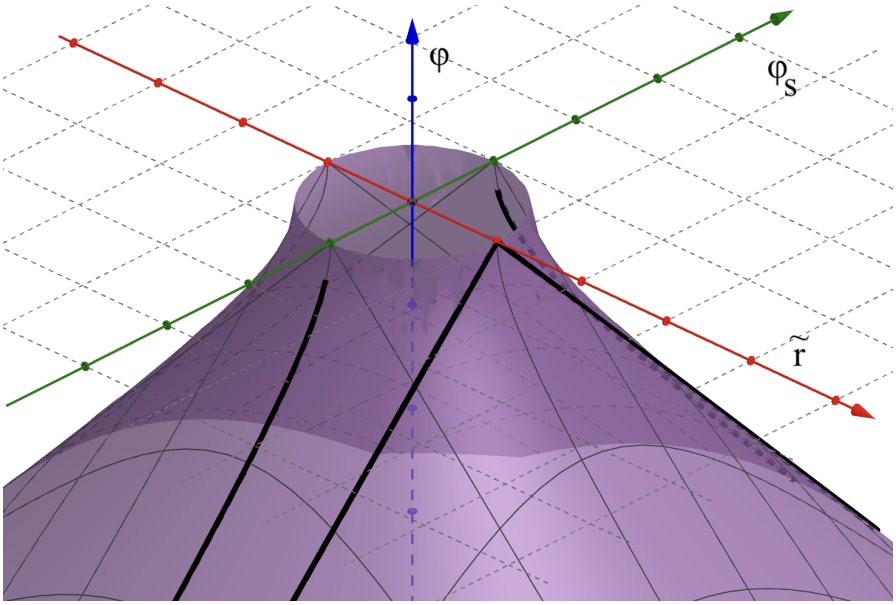

Figure 12: Hyperboloid given by (241) and φ at two values of $\tilde{r}$ (black).

for various φ_s and $\tilde{r} \in [0, \tilde{R}]$ helps us build intuition. From Fig. 9 and 10 we observe that $\varphi(\tilde{r}, \varphi_s)$ is sort of hyperbolic in both $\tilde{r}$ and φ_s. Therefore, we formulate an ansatz

$$a\tilde{r}^2 + b\varphi_s^2 - \varphi^2 = c\,, \tag{240}$$

or equivalently

$$\varphi = -\sqrt{a\tilde{r}^2 + b\varphi_s^2 - c} \tag{241}$$

once we consider only the bottom half of the hyperboloid, and compare with the numerical solution with good qualitative results (see Fig. 11 and 12). Imposing $\varphi(\tilde{R}, \varphi_s) = \varphi_s$ kills two of the three parameters. In details,

$$\varphi(\tilde{R}, \varphi_s) = -\sqrt{a\tilde{R}^2 + b\varphi_s^2 - c} \equiv \varphi_s \to b = 1,\ c = a\tilde{R}^2 \tag{242}$$

and one is left with

$$\varphi = -\sqrt{a(\tilde{r}^2 - \tilde{R}^2) + \varphi_s^2}\,. \tag{243}$$

Since our ansatz was just an approximation, a is not purely numerical, but in itself a function of φ_s. One can see this by fitting (243) over the numerical solution of (239) for different values of φ_s. The results are displayed in Fig. 13. Fitting this plot gives the approximate expression for a

$$a = 0.34 + \frac{1.5 * 10^{-9}}{(\varphi_s + 3.4 * 10^{-4})^2}\,. \tag{244}$$

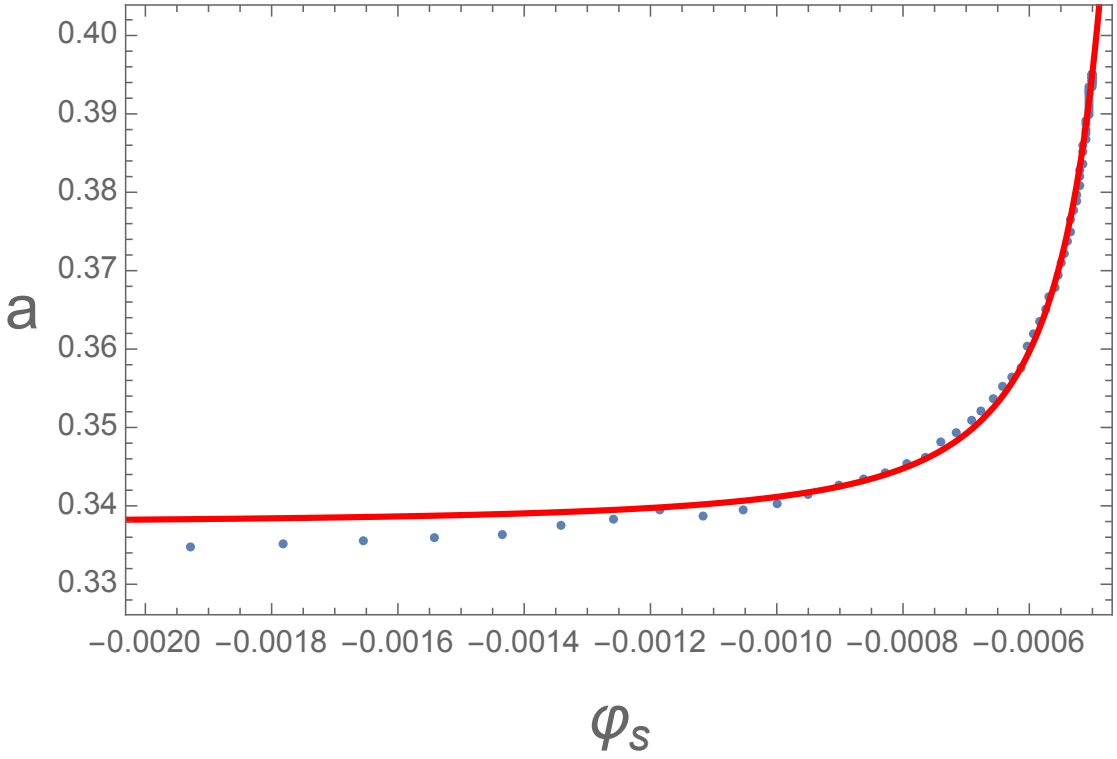

Figure 13: Values of a after fitting (243) over numerical solutions of (239) for various φ_s (blue) and fit (244) (red).

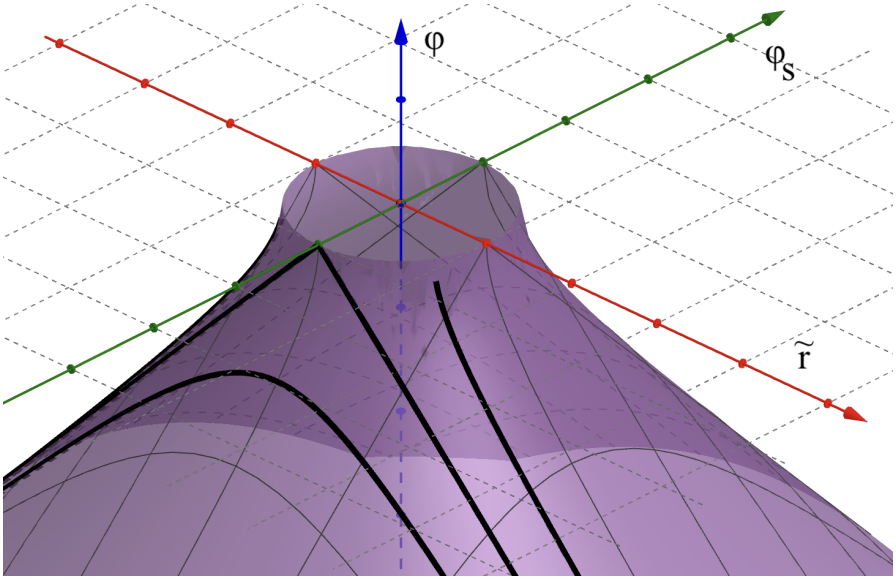

Figure 14: Hyperboloid given by (241) and three φ at fixed φ_s with different qualitative behavior over the domain $\tilde{r} \in [0, \tilde{R}]$ (black).

Let us make some remarks on this result. Numerical solutions of (239) for different φ_s and $\tilde{R}$ reveal a boundary for φ_s at $-\tilde{R}/\sqrt{2}$ (one can also see this in Fig. 13). We can back this up with an analytical argument. Numerically, as φ_s tends to the boundary, $\varphi(\tilde{r}, \varphi_s)$ gets more and more pointy along $\tilde{r}$ (see Fig. 9). The same happens for our ansatz (240) (see Fig. 14). Here one sees even more clearly that when transitioning from a region where φ is defined for every $r \geq 0$ to one where it is not, φ takes the form

$$\varphi = A\tilde{r} + B \,. \tag{245}$$

Surprisingly, this ansatz gives an exact solution for (239) (clearly, we have to drop the constraint $\varphi'(0, \varphi_s) = 0$). By substituting (245) into (239) we find

$$2\tilde{r}A - \frac{\tilde{r}^2}{A\tilde{r} - B} = 0 \,, \tag{246}$$

which is solved by $A = \pm 1/\sqrt{2}$ and $B = 0$. We pick

$$\varphi = -\frac{1}{\sqrt{2}}\tilde{r} \,, \tag{247}$$

since we know $\varphi \equiv \phi - \phi_0 < 0$. Imposing $\varphi(\tilde{R}) = \varphi_s$ gives $\varphi_s = -\tilde{R}/\sqrt{2}$ for this boundary case. Looking back at (243), we notice that it stops being defined at $\tilde{r} = 0$ when $\varphi_s > -\sqrt{a}\tilde{R}$. Therefore, we deduce that for $\varphi_s = -\tilde{R}/\sqrt{2}$, we must have $a = 1/2$.

Let us now look at the horizontal asymptote in Fig. 13, which the raw fit in (244) sets at 0.34. We can show that it corresponds to the region where $\phi/\phi_0 \ll 1$,that is where

$$\mathfrak{g}(\varphi) = \frac{1}{\varphi} = \frac{1}{\phi - \phi 0} \simeq -\frac{1}{\phi_0}\left(1 + \frac{\phi}{\phi_0}\right) \simeq -\frac{1}{\phi_0} \,. \tag{248}$$

In this regime $\mathfrak{g}$ is practically constant, leading us back to the case studied in [1] and in Chapter 3. Taking the derivative of (243) and evaluating at $\tilde{r} = \tilde{R}$ gives

$$\varphi'|_{\tilde{R}} = -\frac{a\tilde{R}}{\sqrt{\varphi_s^2}} = \frac{a\tilde{R}}{\varphi_s} \simeq -\frac{a\tilde{R}}{\phi_0} \,. \tag{249}$$

Comparing it with the constant $\mathfrak{g}$ case (154)

$$\varphi'(\tilde{r})|_{\tilde{R}} = -\frac{1}{\tilde{R}^2}\int_0^{\tilde{R}} d\tilde{r}\tilde{r}^2\frac{1}{\phi_0} = -\frac{\tilde{R}}{3\phi_0} \tag{250}$$

reveals that $a \to 1/3$ for $\phi/\phi_0 \ll 1$. Being $\phi'|_{\tilde{R}}$ the fundamental quantity of this mechanism, we expect the amount of screening L/L_0 to match that of [1] in this limit.

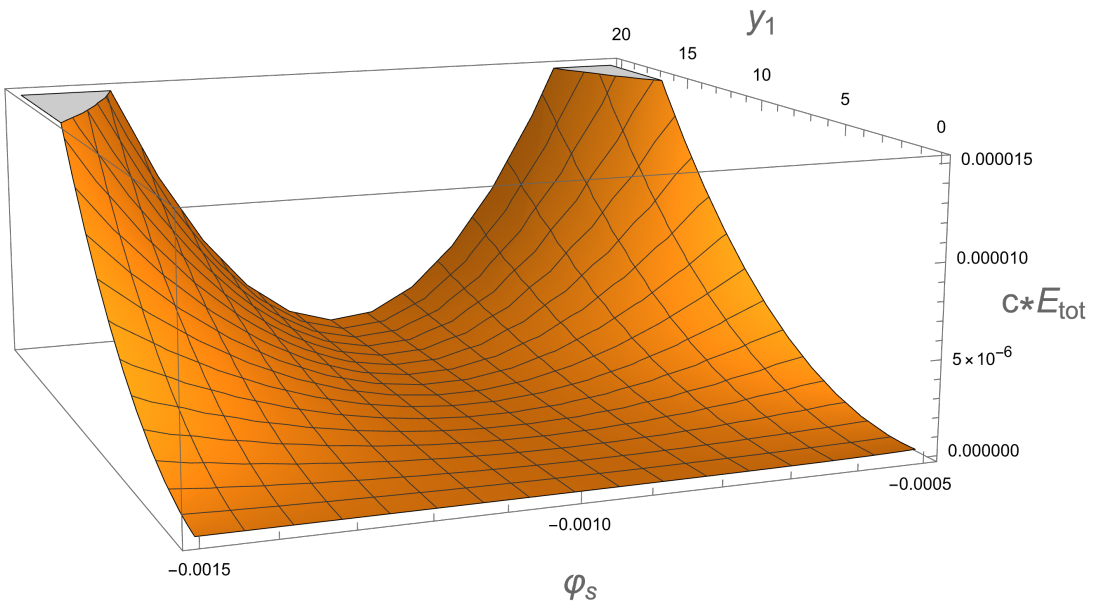

Figure 15: Energy profile E_{tot} for $\phi_0 = 0.001$. Notice how the minimum is close to $\varphi_s = -\phi_0$.

We will verify shortly that this is indeed the case. Imposing the asymptotic value and fitting again, (244) gets updated to

$$a = \frac{1}{3} + \frac{2.5 * 10^{-9}}{(\varphi_s + 3.0 * 10^{-4})^2} \tag{251}$$

and we obtain our final expression for φ

$$\varphi(\tilde{r}, \varphi_s) = -\sqrt{\left(\frac{1}{3} + \frac{2.5 * 10^{-9}}{(\varphi_s + 3.0 * 10^{-4})^2}\right)(\tilde{r}^2 - \tilde{R}^2) + \varphi_s^2}\,. \tag{252}$$

Enforcing the boundary value $a = 1/2$ worsens the fit in the overall domain for the ansatz assumed in (244). Therefore, we prefer not to impose it and label the region $\varphi \sim -\tilde{R}/\sqrt{2}$, i.e. $\phi_0 \sim \tilde{R}/\sqrt{2}$ as not fully trust-worthy.

Plugging (252) into the energy expression (238) give an energy profile (see Fig. 15) that we can minimize numerically with respect to φ_s. This gives us a value for φ_s that we can use in (236). Different values of ϕ_0 and y_1 give different amounts of screening; we sum them up in Fig. 16.

We notice that the bigger ϕ_0 is, the smaller the minimized value of ϕ_s (see Tab. 1). Taking ϕ_s as indicative of the order of magnitude of ϕ in the whole region inside the Sun, we deduce that the ratio ϕ/ϕ_0 can be small even for relatively small values of ϕ_0. We

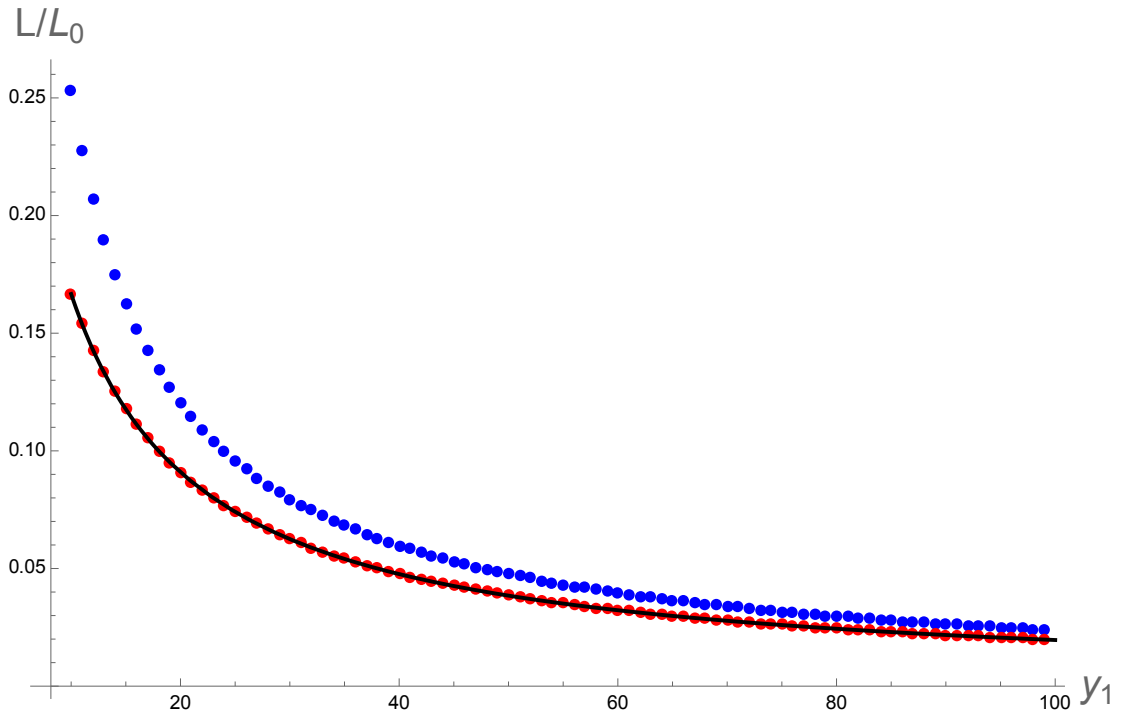

Figure 16: Numerical evaluation of screening for $\phi_0 = 6 * 10^{-4}$ (blue), $\phi_0 = 0.1$ (red) and analytical evaluation for $\mathfrak{g} = const.$ [1] (black).

ϕ_s/ϕ_0	$y_1 = 1$	$y_1 = 10$	$y_1 = 100$
$\phi_0 = 6 * 10^{-4}$	-10^{-1}	$8.5 * 10^{-2}$	10^{-2}
$\phi_0 = 10^{-3}$	$7.0 * 10^{-2}$	$2.9 * 10^{-2}$	$3.3 * 10^{-3}$
$\phi_0 = 10^{-2}$	$1.1 * 10^{-3}$	$2.8 * 10^{-4}$	$3.3 * 10^{-5}$
$\phi_0 = 10^{-1}$	$1.1 * 10^{-5}$	$2.8 * 10^{-6}$	$3.3 * 10^{-7}$

Table 1: ϕ_s/ϕ_0 at the energy minimum for various ϕ_0 and y_1. The top left value being negative indicates that $\phi_s < 0$ and that we cannot trust our analysis in that regime.

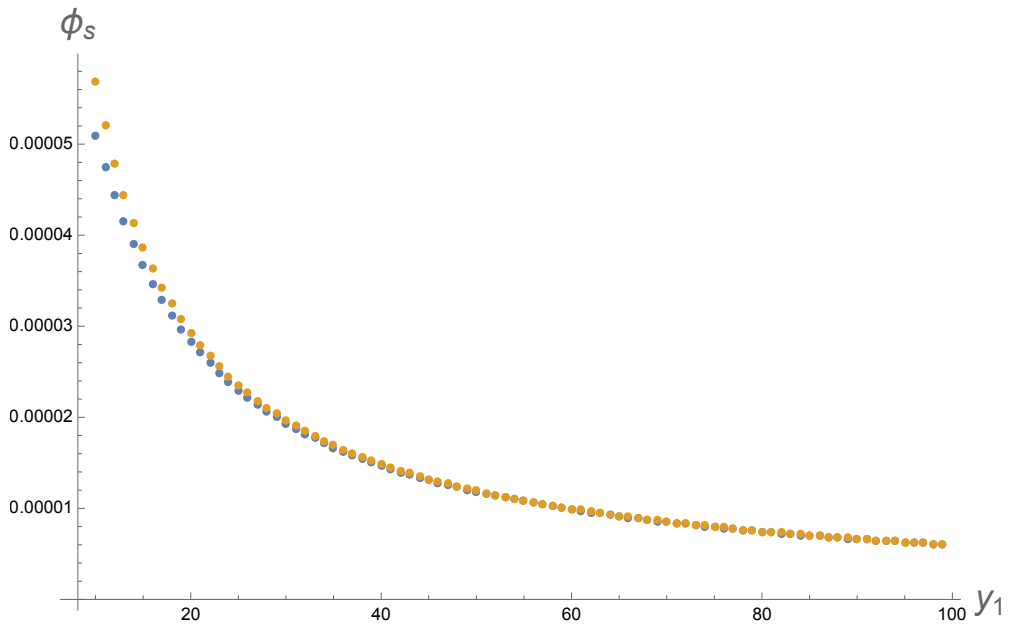

Figure 17: Numerical evaluation of ϕ_s at the energy minimum (blue) compared to the constant $\mathfrak{g}$ case [1] (orange) for $\phi_0 = 6 * 10^{-4}$.

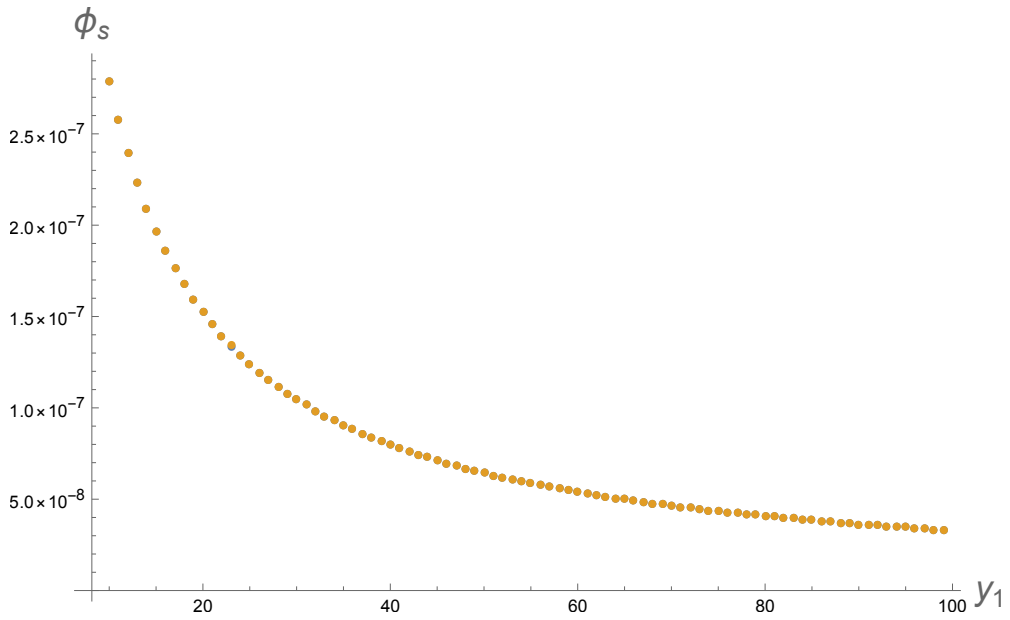

Figure 18: Numerical evaluation of ϕ_s at the energy minimum (blue) compared to the constant $\mathfrak{g}$ case [1] (orange) for $\phi_0 = 0.1$. The overlap is already practically exact.

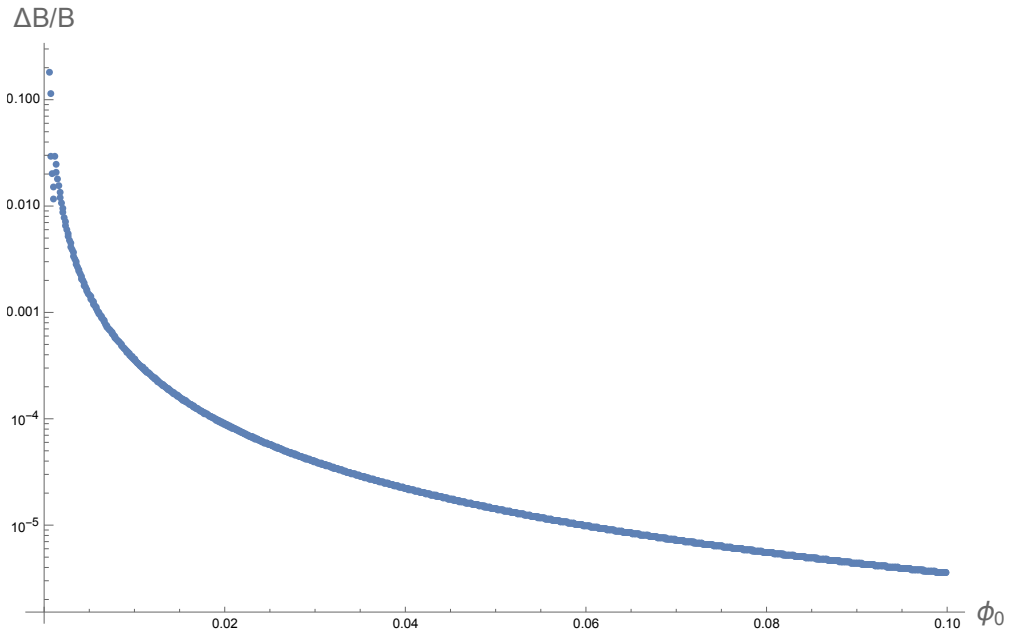

Figure 19: Relative difference between the B resulting from our analysis and the one obtained in [1] where $\mathfrak{g} = const.$ We took $y_1 = 10$.

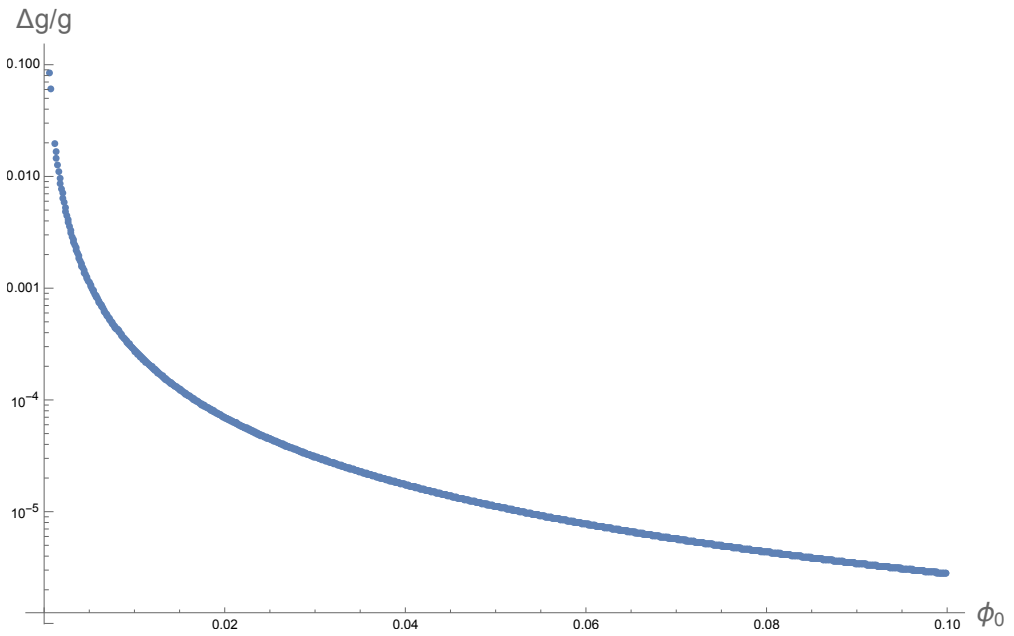

Figure 20: Relative difference between $\mathfrak{g} \sim 1/\varphi_s$ and $\mathfrak{g} = -1/\phi_0$. We took $y_1 = 10$.

see this clearly in Fig 16, where for $\phi_0 = 0.1$ the amount of screening already coincides with the constant $\mathfrak{g}$ case, meaning that the approximation in (248) is allowed.

To be even more certain of the validity of (248) for $\phi/\phi_0 \ll 1$, we compare relevant quantities when evaluated numerically and with the $\mathfrak{g} \simeq -1/\phi_0$ approximation. Results are shown in Fig. 17, 18, 19 and 20. Notice how the approximation gets better as y_1 and ϕ_0 increase.

For constant $\mathfrak{g}$, $L_0 \propto \mathfrak{g}$. This allows us to reinterpret L/L_0 as $\mathfrak{g}_{\text{eff}}/\mathfrak{g}$, where $\mathfrak{g}_{\text{eff}}$ is the effective saxion-SM coupling resulting from the screening. In our model, this is true only when $\phi/\phi_0 \ll 1$. In this regime, we can apply existing experimental constraints to our model (experiments for space-dependent $\mathfrak{g}$ are not as developed yet). In particular, for fifth-forces to evade observation in the solar system, one needs $\mathfrak{g}_{\text{eff}} \lesssim 10^{-3}$; for us this means

$$|\mathfrak{g}_{\text{eff}}| = |\mathfrak{g}|\frac{L}{L_0} \sim \mathcal{O}\left(10^{-3}\right) \ . \tag{253}$$

To study the feasibility of (253), the parameters at our disposal are y_1 and ϕ_0. Recall that the former is itself dependent on the axion gradient Δa and the Sun radius to width thickness ratio R/l. To estimate the order of magnitude of these quantities, one would need a better understanding of the axion potential and of the axion-SM interactions, which we have been neglecting in this thesis. This remains thus an open question in need of further research.

In contrast, ϕ_0 can already be constrained quite accurately. As already mentioned, we know $\varphi_s < -\tilde{R}/\sqrt{2}$. Also, we have been limiting our analysis to the strong warping regime; as a result, we must impose

$$(\rho-\rho_0)^4 \ll \frac{c^4}{\mathcal{V}^{\frac{2}{3}}} = \frac{\frac{27}{4}\pi g_s N(\alpha')^2}{\mathcal{V}^{\frac{2}{3}}} = \frac{\frac{27}{64\pi^3} g_s N l_s^4}{\mathcal{V}^{\frac{2}{3}}} \to \frac{|\rho-\rho_0|}{l_s} < \frac{\left(\frac{27}{64\pi^3} g_s N\right)^{\frac{1}{4}}}{\mathcal{V}^{\frac{1}{6}}} \ . \tag{254}$$

Recalling (196) we find

$$\varphi = \sqrt{\frac{\mathcal{V}^{\frac{1}{3}}}{2g_s\mathcal{V}_W}}\frac{\rho-\rho_0}{l_s} \sim \frac{1}{\sqrt{2g_s}\mathcal{V}^{\frac{1}{3}}}\frac{(\rho-\rho_0)}{l_s} \ , \tag{255}$$

where we used

$$\mathcal{V} \sim \mathcal{V}_W \ , \tag{256}$$

which is true if we assume the conifold to be a small part of the overall Calabi-Yau. Combining (254) and (255) we find

$$|\varphi| < \frac{1}{\sqrt{2g_s}\mathcal{V}^{\frac{1}{3}}}\frac{\left(\frac{27}{64\pi^3} g_s N\right)^{\frac{1}{4}}}{\mathcal{V}^{\frac{1}{6}}} \sim \frac{\left(\frac{N}{g_s}\right)^{\frac{1}{4}}}{4\mathcal{V}^{\frac{1}{2}}} \ . \tag{257}$$

Overall

$$-\frac{\left(\frac{N}{g_s}\right)^{\frac{1}{4}}}{4\mathcal{V}^{\frac{1}{2}}} < \varphi < -\frac{\tilde{R}}{\sqrt{2}} \simeq -5 * 10^{-4} \,. \tag{258}$$

Recalling that $\varphi \sim -\phi_0$, our constraints on ϕ_0 are

$$\frac{\tilde{R}}{\sqrt{2}} \simeq 5 * 10^{-4} < \phi_0 < \frac{\left(\frac{N}{g_s}\right)^{\frac{1}{4}}}{4\mathcal{V}^{\frac{1}{2}}} \,. \tag{259}$$

Notice how we also get constraints on $\mathcal{V}$ from

$$5 * 10^{-4} < \frac{\left(\frac{N}{g_s}\right)^{\frac{1}{4}}}{4\mathcal{V}^{\frac{1}{2}}} \to 1 \lesssim \mathcal{V} \lesssim 10^6 \left(\frac{N}{g_s}\right)^{\frac{1}{2}} \,. \tag{260}$$

These allow a bit of overlap with the LVS regime, which is good news if one hopes to stabilize the stringy moduli. However, one should remember that the volume upper boundary is just the result of us limiting the model to the strong warping regime. It is therefore worth it to attempt a generalization of our research beyond this regime, in the hope of extending the axio-chameleon screening mechanism well inside LVS.

5 Conclusion

We analyzed possible implementations of the novel axio-chameleon screening mechanism in Type IIB String Theory. While closed-string moduli seem unable to recreate such effect, brane-position moduly showed promising results.

We assumed the Standard Model to live on a D3/$\overline{\text{D3}}$-brane on a warped deformed conifold. By using the radial coordinate and a combination of the angular coordinates of the brane as a saxion-axion pair, screening can be achieved only for a warp factor that decreases with the radial coordinate. For this reason, we assumed a stack of branes to be fixed further away from the tip than the SM-brane. The saxion-SM coupling approaches a constant value the further the stack is from the tip.

Since we limited ourselves to the strong warping regime, we obtained a constraint on the compactified volumes that lets us barely reach LVS. However, currently there is no reason to believe this constraint could not the relaxed in the future.

We also acknowledge the necessity for further research in the study of the saxion and axion potentials and the axion-SM interactions. In particular, managing to recreate a slow-roll saxion potential in this non-conventional brane setup would solidify our model. Also, throughout this thesis we have assumed that one can create an axion from a combination of the angular brane-position moduli. This needs to be verified via a detailed study of the field potential and its interaction with the SM.

Acknowledgements

I am grateful to Prof. Susha Louise Parameswaran and Prof. Michele Cicoli for the advice and guidance provided during this months. I also acknowledge and thank Joaquim Gomes and Kajal Singh for the many constructive conversations that helped in the realization of this thesis.

Appendix

A Review on Quintessence

Various models use the radial coordinate of a D3/$\overline{\text{D3}}$-brane as a quintessence field in an attempt of explaining the observed current accelerated expansion of the universe. The stringy embedding of the axio-chameleon screening mechanism we proposed could be used in this context, relaxing experimental constraints on quintessence fifth-forces. For this reason, we provide here a short overview on the topic.

To describe an expanding universe, one must introduce a time-dependent scale factor in the metric. This is the role of $a(t)$ in the FLRW metric

$$ds^2 = -dt^2 + a^2(t)d\mathbf{x}^2 = -dt^2 + a^2(t)\left(dr^2 + r^2 d\Omega^2\right) \,, \tag{261}$$

where the time coordinate is absolute, but the spatial ones are comoving with the expansion. The maximum comoving distance a particle can travel in an interval of time, known as the particle horizon, is given by

$$\Delta r = \int_{r_1}^{r_2} dr = \int_{t_1}^{t_2} \frac{dt}{a(t)} = \int_{t_1}^{t_2} \frac{da}{a^2(t)}\frac{dt}{da}a(t) = \int_{t_1}^{t_2} \frac{d(\ln a)}{aH} \,, \tag{262}$$

where we obviously considered a massless particle ($ds^2 = 0$) and defined the Hubble parameter as

$$H \equiv \frac{1}{a}\frac{da}{dt} \,. \tag{263}$$

For the horizon to be shrinking as we observe today, the comoving Hubble radius $(aH)^{-1}$ must be negative, i.e.

$$\frac{d}{dt}\frac{1}{aH} = -\frac{1}{a}\left(\frac{\dot{H}}{H^2} + 1\right) < 0 \,, \tag{264}$$

which is equivalent to

$$\varepsilon \equiv -\frac{\dot{H}}{H^2} < 1 \,. \tag{265}$$

We will now show that (265) can be achieved from a scalar field, which is referred to as quintessence, living in the FLRW spacetime. Let us start from the action

$$S = \int d^4x\sqrt{-g}\left(\frac{M_p^2}{2}R - \frac{M_p^2}{2}(\partial\phi)^2 - V(\phi)\right) \,, \tag{266}$$

where we are using the FLRW metric. The Variational Principle gives the Klein-Gordon equation with Hubble friction

$$\ddot{\phi} + 3H\dot{\phi} = -\frac{\partial_\phi V}{M_p^2} \,, \tag{267}$$

while the Friedmann equation is

$$3H^2 = \frac{1}{2}\dot{\phi}^2 + \frac{V}{M_p^2} \,. \tag{268}$$

Differentiating (268) with respect to time gives

$$\partial_t(H^2) = 2H\dot{H} = \frac{1}{3}\dot{\phi}\ddot{\phi} + \frac{1}{3}\frac{\partial_\phi V}{M_p^2}\dot{\phi} \,. \tag{269}$$

By substituting $\partial_\phi V/M_p^2$ with (267) we find

$$\dot{H} = \frac{1}{2}\dot{\phi}^2 \tag{270}$$

and consequently (265) turns into

$$\varepsilon = \frac{\frac{1}{2}\dot{\phi}^2}{H^2} = \frac{\frac{3}{2}\dot{\phi}^2}{\frac{1}{2}\dot{\phi}^2 + \frac{V}{M_p^2}} \xrightarrow{V/M_p^2 \gg \frac{1}{2}\dot{\phi}^2} 0 \,. \tag{271}$$

In the limit we took in (271), (265) is satisfied. This can happen in a number of potentials, one of the most famous families being the slow-roll ones. These are characterized by a very small slope, so that the kinetic energy of the field is indeed subleading to the potential.

B Fictitious Non-Linear Sigma Models

Non-linear sigma models are characterized by a generalized kinetic term, responsible for interactions between the scalar fields. However, there are instances when these interactions are just artifacts of a poor choice of fields and an appropriate redefinition can lead us back to a linear sigma model. Here we will argue that the action

$$S = \frac{M_p^2}{2}\int d^4x\sqrt{-g}\left(R - \partial_\mu\phi\partial^\mu\phi - \phi^2\partial_\mu a\partial^\mu a\right) \tag{272}$$

falls into this category. Our interest in (272) is justified by its similarity with (200), which coincides for $f = M_p$.

The target-space metric in (272) is

$$\mathcal{G}_{ab} = \begin{pmatrix} 1 & 0 \\ 0 & \phi^2 \end{pmatrix} , \tag{273}$$

which we recognize as the 2D flat metric in polar coordinates. Therefore, applying the polar-cartesian coordinate conversion

$$\begin{aligned} \phi^2 &= \chi^2 + \theta^2 \, , \\ \tan a &= \frac{\theta}{\chi} \end{aligned} \tag{274}$$

is guaranteed to turn (272) into the equivalent linear sigma model

$$S = \frac{M_p^2}{2} \int d^4x \sqrt{-g} \left(R - \partial_\mu \chi \partial^\mu \chi - \partial_\mu \theta \partial^\mu \theta \right) \, , \tag{275}$$

where the fictitious interactions vanished.

One can make even further observations in the framework of Supergravity. Let us start from a Kähler potential

$$K = 2n^2 \Phi \bar{\Phi} \, , \tag{276}$$

which originates the metric

$$\mathcal{G}_{ab} = K_{\Phi\bar{\Phi}} = 2n^2 \tag{277}$$

appearing in the Supergravity lagrangian term [34]

$$L \supset -\sqrt{-g} M_p^2 K_{\Phi\bar{\Phi}} \partial_\mu \Phi \partial^\mu \bar{\Phi} \, . \tag{278}$$

To express this in term of real fields, one needs to choose how to split the complex field Φ. Picking $\Phi = \chi + i\theta$ or $\Phi = \phi \exp(ia)$ gives

$$L \supset -\sqrt{-g} M_p^2 2n^2 \left(\partial_\mu \chi \partial^\mu \chi + \partial_\mu \theta \partial^\mu \theta \right) \tag{279}$$

or

$$L \supset -\sqrt{-g} M_p^2 2n^2 \left(\partial_\mu \phi \partial^\mu \phi + \phi^2 \partial_\mu a \partial^\mu a \right) \tag{280}$$

respectively. Despite the minimalist appeal of (279), recalling that K appears in the scalar potential

$$V = M_p^4 e^G \left(G^{\Phi\bar{\Phi}} G_\Phi G_{\bar{\Phi}} - 3 \right) , \quad G \equiv K + \ln |W|^2 \tag{281}$$

might hint us towards the polar decomposition, since K would be independent of a, making $\{\phi, a\}$ a promising saxion-axion pair. However, Kähler invariance

$$\begin{aligned} K &\mapsto K + f(\Phi) + \bar{f}(\bar{\Phi}) \, , \\ W &\mapsto e^{-f(\Phi)} W \end{aligned} \tag{282}$$

tells us that (276) is equivalent to

$$K = 2n^2\Phi\bar{\Phi} + (n\Phi)^2 + (n\bar{\Phi})^2 = n^2(\Phi + \bar{\Phi})^2 \,, \tag{283}$$

which seems to suggest $\{\chi, \theta\}$ as a saxion-axion pair.

Based on these considerations, we conclude that (279) and (280) are indeed equivalent and that information on the eventual axionic nature of a field can only come from W.

References

[1] Philippe Brax, C. P. Burgess, and F. Quevedo. "Axio-Chameleons: a novel string-friendly multi-field screening mechanism". In: *JCAP* 03 (2024), p. 015. DOI: 10.1088/1475-7516/2024/03/015. arXiv: 2310.02092 [hep-th].

[2] Daniel Baumann and Liam McAllister. *Inflation and String Theory*. Cambridge Monographs on Mathematical Physics. Cambridge University Press, May 2015. ISBN: 978-1-107-08969-3, 978-1-316-23718-2. DOI: 10.1017/CBO9781316105733. arXiv: 1404.2601 [hep-th].

[3] Bruno Valeixo Bento et al. "A new de Sitter solution with a weakly warped deformed conifold". In: *JHEP* 12 (2021), p. 124. DOI: 10.1007/JHEP12(2021)124. arXiv: 2105.03370 [hep-th].

[4] Michele Cicoli et al. "Back to the origins of brane–antibrane inflation". In: *Eur. Phys. J. C* 85.3 (2025), p. 315. DOI: 10.1140/epjc/s10052-025-13982-9. arXiv: 2410.00097 [hep-th].

[5] Ofer Aharony, Yaron E. Antebi, and Micha Berkooz. "Open string moduli in Kachru-Kallosh-Linde-Trivedi compactifications". In: *Phys. Rev. D* 72 (10 Nov. 2005), p. 106009. DOI: 10.1103/PhysRevD.72.106009. URL: https://link.aps.org/doi/10.1103/PhysRevD.72.106009.

[6] Roy Maartens and Kazuya Koyama. "Brane-World Gravity". In: *Living Rev. Rel.* 13 (2010), p. 5. DOI: 10.12942/lrr-2010-5. arXiv: 1004.3962 [hep-th].

[7] Tomi Koivisto, Danielle Wills, and Ivonne Zavala. "Dark D-brane Cosmology". In: *JCAP* 06 (2014), p. 036. DOI: 10.1088/1475-7516/2014/06/036. arXiv: 1312.2597 [hep-th].

[8] Jeremy Sakstein. "Disformal Theories of Gravity: From the Solar System to Cosmology". In: *JCAP* 12 (2014), p. 012. DOI: 10.1088/1475-7516/2014/12/012. arXiv: 1409.1734 [astro-ph.CO].

[9] Philippe Brax and Clare Burrage. "Constraining Disformally Coupled Scalar Fields". In: *Phys. Rev. D* 90.10 (2014), p. 104009. DOI: 10.1103/PhysRevD.90.104009. arXiv: 1407.1861 [astro-ph.CO].

[10] Michele Cicoli et al. "String cosmology: From the early universe to today". In: *Phys. Rept.* 1059 (2024), pp. 1–155. DOI: 10.1016/j.physrep.2024.01.002. arXiv: 2303.04819 [hep-th].

[11] Philip Candelas and Xenia C. de la Ossa. "Comments on Conifolds". In: *Nucl. Phys. B* 342 (1990), pp. 246–268. DOI: 10.1016/0550-3213(90)90577-Z.

[12] URL: https://en.wikipedia.org/wiki/Conifold.

[13] Leopoldo A. Pando Zayas and Arkady A. Tseytlin. "3-branes on resolved conifold". In: *JHEP* 11 (2000), p. 028. DOI: 10.1088/1126-6708/2000/11/028. arXiv: hep-th/0010088.

[14] Igor R. Klebanov and Matthew J. Strassler. "Supergravity and a confining gauge theory: Duality cascades and chi SB resolution of naked singularities". In: *JHEP* 08 (2000), p. 052. DOI: 10.1088/1126-6708/2000/08/052. arXiv: hep-th/0007191.

[15] Igor R. Klebanov and Arkady A. Tseytlin. "Gravity duals of supersymmetric SU(N) x SU(N+M) gauge theories". In: *Nucl. Phys. B* 578 (2000), pp. 123–138. DOI: 10.1016/S0550-3213(00)00206-6. arXiv: hep-th/0002159.

[16] Luis E. Ibanez and Angel M. Uranga. *String theory and particle physics: An introduction to string phenomenology*. Cambridge University Press, Feb. 2012. ISBN: 978-0-521-51752-2, 978-1-139-22742-1.

[17] Steven B. Giddings, Shamit Kachru, and Joseph Polchinski. "Hierarchies from fluxes in string compactifications". In: *Phys. Rev. D* 66 (2002), p. 106006. DOI: 10.1103/PhysRevD.66.106006. arXiv: hep-th/0105097.

[18] Michael R. Douglas, Jessie Shelton, and Gonzalo Torroba. "Warping and supersymmetry breaking". In: (Apr. 2007). arXiv: 0704.4001 [hep-th].

[19] K. S. Stelle. "BPS branes in supergravity". In: *ICTP Summer School in High-energy Physics and Cosmology*. Mar. 1998. arXiv: hep-th/9803116.

[20] C. Brans and R. H. Dicke. "Mach's principle and a relativistic theory of gravitation". In: *Phys. Rev.* 124 (1961). Ed. by Jong-Ping Hsu and D. Fine, pp. 925–935. DOI: 10.1103/PhysRev.124.925.

[21] Khaled Saaidi, Abolhassan Mohammadi, and Haidar Sheikhahmadi. "γ Parameter and Solar System constraint in Chameleon Brans Dick theory". In: *Phys. Rev. D* 83 (2011), p. 104019. DOI: 10.1103/PhysRevD.83.104019. arXiv: 1201.0271 [gr-qc].

[22] Carla R. Almeida, Olesya Galkina, and Julio César Fabris. "Quantum and Classical Cosmology in the Brans–Dicke Theory". In: *Universe* 7.8 (2021), p. 286. DOI: 10.3390/universe7080286. arXiv: 2106.14299 [gr-qc].

[23] Adam Smith et al. "A Minimal Axio-dilaton Dark Sector". In: (Oct. 2024). arXiv: 2410.11099 [hep-th].

[24] C. P. Burgess and F. Quevedo. "Axion homeopathy: screening dilaton interactions". In: *JCAP* 04.04 (2022), p. 007. DOI: 10.1088/1475-7516/2022/04/007. arXiv: 2110.10352 [hep-th].

[25] Clare Burrage and Jeremy Sakstein. “Tests of Chameleon Gravity”. In: *Living Rev. Rel.* 21.1 (2018), p. 1. DOI: 10.1007/s41114-018-0011-x. arXiv: 1709.09071 [astro-ph.CO].

[26] Loukas Grafakos. *Classical Fourier Analysis*. 2nd ed. Vol. 249. Graduate Texts in Mathematics. New York: Springer, 2008.

[27] Austin Joyce et al. “Beyond the Cosmological Standard Model”. In: *Phys. Rept.* 568 (2015), pp. 1–98. DOI: 10.1016/j.physrep.2014.12.002. arXiv: 1407.0059 [astro-ph.CO].

[28] D. J. Kapner et al. “Tests of the Gravitational Inverse-Square Law below the Dark-Energy Length Scale”. In: *Phys. Rev. Lett.* 98 (2 Jan. 2007), p. 021101. DOI: 10.1103/PhysRevLett.98.021101. URL: https://link.aps.org/doi/10.1103/PhysRevLett.98.021101.

[29] E. G. Adelberger et al. “Particle-Physics Implications of a Recent Test of the Gravitational Inverse-Square Law”. In: *Phys. Rev. Lett.* 98 (13 Mar. 2007), p. 131104. DOI: 10.1103/PhysRevLett.98.131104. URL: https://link.aps.org/doi/10.1103/PhysRevLett.98.131104.

[30] Amol Upadhye, Wayne Hu, and Justin Khoury. “Quantum Stability of Chameleon Field Theories”. In: *Phys. Rev. Lett.* 109 (2012), p. 041301. DOI: 10.1103/PhysRevLett.109.041301. arXiv: 1204.3906 [hep-ph].

[31] Steven Weinberg. *The quantum theory of fields. Vol. 2: Modern applications*. Cambridge University Press, Aug. 2013. ISBN: 978-1-139-63247-8, 978-0-521-67054-8, 978-0-521-55002-4. DOI: 10.1017/CBO9781139644174.

[32] Adam Smith et al. “CMB implications of multi-field axio-dilaton cosmology”. In: *JCAP* 12 (2024), p. 058. DOI: 10.1088/1475-7516/2024/12/058. arXiv: 2408.10820 [hep-th].

[33] Paulo C. C. Freire et al. “The relativistic pulsar-white dwarf binary PSR J1738+0333 II. The most stringent test of scalar-tensor gravity”. In: *Mon. Not. Roy. Astron. Soc.* 423 (2012), p. 3328. DOI: 10.1111/j.1365-2966.2012.21253.x. arXiv: 1205.1450 [astro-ph.GA].

[34] D. G. Cerdeno and C. Munoz. “An introduction to supergravity”. In: *PoS* CORFU98 (1998). Ed. by G. Zoupanos et al., p. 011. DOI: 10.22323/1.001.0011.

[35] C. P. Burgess, Danielle Dineen, and F. Quevedo. “Yoga Dark Energy: natural relaxation and other dark implications of a supersymmetric gravity sector”. In: *JCAP* 03.03 (2022), p. 064. DOI: 10.1088/1475-7516/2022/03/064. arXiv: 2111.07286 [hep-th].

[36] C. P. Burgess et al. “The Inflationary brane anti-brane universe”. In: *JHEP* 07 (2001), p. 047. DOI: 10.1088/1126-6708/2001/07/047. arXiv: hep-th/0105204.

[37] G. R. Dvali, Q. Shafi, and S. Solganik. “D-brane inflation”. In: *4th European Meeting From the Planck Scale to the Electroweak Scale*. May 2001. arXiv: hep-th/0105203.

[38] Shamit Kachru et al. “Towards inflation in string theory”. In: *JCAP* 10 (2003), p. 013. DOI: 10.1088/1475-7516/2003/10/013. arXiv: hep-th/0308055.

[39] Bruno Valeixo Bento et al. “Dark Energy in String Theory”. In: *PoS* CORFU2019 (2020), p. 123. DOI: 10.22323/1.376.0123. arXiv: 2005.10168 [hep-th].

[40] Daniel Baumann et al. “On D3-brane Potentials in Compactifications with Fluxes and Wrapped D-branes”. In: *JHEP* 11 (2006), p. 031. DOI: 10.1088/1126-6708/2006/11/031. arXiv: hep-th/0607050.